AGU PUBLICATIONS

JGR

Journal of Geophysical Research: Oceans

RESEARCH ARTICLE

10.1002/2015JC011232

Special Section:
Forum for Arctic Modeling and Observational Synthesis (FAMOS): Results and Synthesis of Coordinated Experiments

The future of the subsurface chlorophyll-a maximum in the Canada Basin—A model intercomparison

N. S. Steiner[1,2], T. Sou[1], C. Deal[3], J. M. Jackson[4], M. Jin[3], E. Popova[5], W. Williams[1], and A. Yool[5]

[1]Fisheries and Oceans Canada, Institute of Ocean Sciences, Sidney, British Columbia, Canada, [2]Canadian Centre for Climate Modelling and Analysis, Environment Canada, Victoria, British Columbia, Canada, [3]International Arctic Research Center, University of Alaska Fairbanks, Fairbanks, Alaska, USA, [4]ASL Environmental Sciences, Saanichton, British Columbia, Canada, [5]National Oceanographic Center, Southampton, UK

Abstract Six Earth system models and three ocean-ice-ecosystem models are analyzed to evaluate magnitude and depth of the subsurface Chl-*a* maximum (SCM) in the Canada Basin and ratio of surface to subsurface Chl-*a* in a future climate scenario. Differences in simulated Chl-a are caused by large intermodel differences in available nitrate in the Arctic Ocean and to some extent by ecosystem complexity. Most models reproduce the observed SCM and nitracline deepening and indicate a continued deepening in the future until the models reach a new state with seasonal ice-free waters. Models not representing a SCM show either too much nitrate and hence no surface limitation or too little nitrate with limited surface growth only. The models suggest that suppression of the nitracline and deepening of the SCM are caused by enhanced stratification, likely driven by enhanced Ekman convergence and freshwater contributions with primarily large-scale atmospheric driving mechanisms. The simulated ratio of near-surface Chl-*a* to depth-integrated Chl-*a* is slightly decreasing in most areas of the Arctic Ocean due to enhanced contributions of subsurface Chl-*a*. Exceptions are some shelf areas and regions where the continued ice thinning leaves winter ice too thin to provide a barrier to momentum fluxes, allowing winter mixing to break up the strong stratification. Results confirm that algorithms determining vertically integrated Chl-*a* from surface Chl-*a* need to be tuned to Arctic conditions, but likely require little or no adjustments in the future.

Key Points:
- Model simulations suggest the observed SCM deepening to continue in the future
- Differences in projected SCM deepening are caused by physical factors
- Algorithms for integrated Chl-*a* require Arctic setting, but little future change

Supporting Information:
- Supporting Information S1
- Figure S1
- Figure S2
- Figure S3
- Figure S4
- Figure S5

Correspondence to:
N. S. Steiner,
nadja.steiner@ec.gc.ca

Citation:
Steiner, N. S., T. Sou, C. Deal, J. M. Jackson, M. Jin, E. Popova, W. Williams, and A. Yool (2016), The future of the subsurface chlorophyll-a maximum in the Canada Basin—A model intercomparison, *J. Geophys. Res. Oceans*, *121*, 387–409, doi:10.1002/2015JC011232.

Received 12 AUG 2015
Accepted 8 DEC 2015
Accepted article online 14 DEC 2015
Published online 11 JAN 2016

1. Introduction

Subsurface chlorophyll-a maxima (SCMs) are a common feature in the Arctic Ocean during the post-bloom period when surface chlorophyll-a (Chl-*a*) concentration is low ($<$0.5 mg m^{-3}) [*Ardyna et al*., 2013] and can contribute significantly to the vertically integrated Chl-*a* concentration. SCMs develop every summer after the water column stratifies and surface nutrients have been used up. Phytoplankton within the SCM causes the nitracline to deepen during the growth season by exhausting the nitrate (NO_3) above. The SCM settles to a depth where light remains sufficient to support growth. There the SCM acts as a boundary, preventing the upward diffusion of NO_3 into the upper euphotic zone [*Tremblay et al*., 2008; *Mundy et al*., 2009]. Hence, SCMs are frequently located below the pycnocline [e.g., *Martin et al*., 2010], and often are correlated with the euphotic and nitracline depths [*Martin et al*., 2010; *Brown et al*., 2015]. As the euphotic depth shallows toward the end of the growing season, extreme light limitation, potentially triggered by sea ice growth, may cause the SCM community to die off and sink to the ocean floor [*Brown et al*., 2015].

The seasonal evolution, vertical extension, productivity, and assemblage composition varies regionally and is influenced by stratification, nutrients, and source water masses [e.g., *Martin et al*., 2010; *Brown et al*., 2015]. The SCM tends to be shallower on the shelves (e.g., 30 m in the Chukchi Sea compared to 50–60 m in the Canada Basin) [*Brown et al*., 2015]. *Martin et al*. [2010] found the SCM absent only near rivers and in shallow regions where mixing and upwelling are important. The SCM in the western Arctic is associated with the inflow of Pacific summer (PSW) and winter waters (PWW). These waters are rich in nutrients and generally stay below the fresher and nutrient-depleted near-surface waters [*Carmack et al*., 1989, 2004]. *Monier et al*. [2014] suggest the SCM maintenance may be highly susceptible to changes in the physical structure of the water column, e.g., the displacement of Pacific water to greater depth and contributions of terrigenous material. *Lovejoy* [2012] and *Li et al*. [2009] indicate that any disruption of the fragile light-nutrient

Table 1. Description of Model Ocean-Ecosystem Components

Model	Dimensions[a] (Ocean: x-y-z)	Ecosystem[b]	Chl-*a*	Forcing[c]	References
CanESM2	256 × 192 × 40	NPZ	Variable Chl-*a*:N		*Arora et al.* [2011], *Christian et al.* [2010], and *Zahariev et al.* [2008]
GFDL-ESM2M	360 × 200 × 50	N4P3	Variable Chl-*a*:C		*Dunne et al.* [2012, 2013]
HadGEM2-ES	360 × 216 × 40	N3P2Z	Constant Chl-*a*:C		*HadGEM2 DevelopmenTeam* [2011], *Collins et al.* [2011], and *Palmer and Totterdell* [2001]
IPSL-CM5A-LR	182 × 149 × 31	N5P2Z2	Variable Chl-*a*:C		*Dufresne et al.* [2013] and *Aumont et al.* [2003]
MPI-ESM-LR	256 × 220 × 40	N3PZ	Constant Chl-*a*:C		*Giorgetta et al.* [2013], *Ilyina et al.* [2013], and *Six and Maier-Reimer* [1996]
MIROC-ESM	256 × 192 × 44	NPZ	Constant Chl-*a*:C		*Watanabe et al.* [2011], *Kawamiya et al.* [2000], and *Oschlies* [2001]
LANL-UAF	384 × 320 × 40	N4P3Z2	Variable Chl-*a*:C	GFDL-ESM2M	*Jin et al.* [2012a,b] and *Moore et al.* [2002]
NEMO-MEDUSA	1442 × 1021 × 64	N3P2Z2	Variable Chl-*a*:N	HadGEM2-ES	*Yool et al.* [2013a] and *Popova et al.* [2014]
NAA-CMOC[d]	568 × 400 × 46[e]	NPZ	Variable Chl-*a*:N	CanRCM4+CanESM2	*Hu and Myers* [2013, 2014] and *Zahariev et al.* [2008]

[a]Number of grid points in the horizontal (x,y) and vertical (z), reflecting horizontal resolutions ranging from 0.3 to 1° to a maximum of 2°.
[b]Ecosystem complexities are indicated via numbers of nutrient (N), phytoplankton (P), and zooplankton (Z) groups.
[c]Model providing atmospheric forcing (HROMs only) and ocean boundary conditions (NAA-CMOC only).
[d]Regional model covering the Arctic.

balance at the SCM might alter the community structure. Observations from 2003 to 2012 show a deepening of the nitracline and the SCM over time [*McLaughlin and Carmack*, 2010]. In this study, we will use a selection of Earth System Models (ESMs) and higher-resolution ocean models (indicated in Table 1) to evaluate whether these models are able to represent the observed vertical Chl-*a* distribution and trend in the Canada Basin and to analyze the temporal evolution of the SCM in future projections. In addition, we will evaluate changes in the ratio of near-surface to integrated Chl-*a*.

2. Background

2.1. Arctic Physical Oceanography

The Arctic Ocean can be divided into two different water mass assemblies [*McLaughlin et al.*, 1996]. In the eastern Arctic (Nansen and Amundsen Basins), the water mass assembly is characterized by the absence of Pacific water and warmer Atlantic water. In the western Arctic (Canada and Makarov Basins), the water mass assembly is characterized by the presence of Pacific water and colder Atlantic water. The front between the eastern and western Arctic varies on interannual time scales [*McLaughlin et al.*, 2002; *Alkire et al.*, 2015]. The western Arctic is much fresher than the eastern Arctic, resulting in shallower surface mixed layers in the western Arctic. Using observations from 1979 to 2012, *Peralta-Ferriz and Woodgate* [2015] found that the average maximum winter mixed-layer depth (MLD) is 33.1 m in the Canada Basin and 72.5 m in the Eurasian Basin. In summer, the average minimum MLD is 8.9 m in the Canada Basin and 22.3 m in the Eurasian Basin. In the Canada Basin, increased stratification from sea ice melt, river runoff [*Maykut and McPhee*, 1995; *Jackson et al.*, 2010a] or from the collapse of submesoscale fronts [*Timmermans et al.*, 2012] causes the surface mixed layer to shoal in June or July. The increased stratification can trap incoming solar radiation below the surface mixed layer forming a near-surface temperature maximum at typical depths of 10–30 m (NSTM) [*Jackson et al.*, 2010b]. In the fall and winter, increased kinetic energy can decrease stratification, causing the NSTM to be entrained into the surface mixed layer. During some winters, stratification is stronger than kinetic energy, which causes the NSTM to be stored throughout the winter, where it can periodically melt the bottom of sea ice [*Jackson et al.*, 2012; *Timmermans*, 2015]. The NSTM also forms in the Eurasian Basin in summer but weaker stratification causes it to disappear in fall [*Polyakov et al.*, 2013]. Pacific water is found below the remnant winter mixed layer in the

Canada Basin, at typical depths of about 40–200 m [*Steele et al*., 2004]. Recent research has shown that between 2003 and 2013, the Pacific water layer thickened and freshened [*Timmermans et al*., 2014]. The changes to nutrient-rich Pacific layer influence the depth of the SCM, which normally coincides with the top of the Pacific water [*Jackson et al*., 2010a; *McLaughlin and Carmack*, 2010]. More specifically, *McLaughlin and Carmack* [2010] suggested that in the Canada Basin, recent increases in Ekman convergence lead to enhanced freshwater content, a deepening of the nitracline and the SCM. The nitracline deepening was found to be the main cause for the SCM deepening (at a rate of 3.2 m yr^{-1}) [*Jackson et al*., 2010a]. *McLaughlin and Carmack* [2010] also found a decrease in NO_3 concentrations at the SCM depth and suggest that the availability of light may play a progressively greater role in determining the depth at which primary production (PP) occurs. Additional increases in freshwater input related to sea ice melt and river runoff [*McPhee et al*., 2009; *Rabe et al*., 2011] lead to an enhanced salinity stratification constraining the vertical heat flux and nutrient renewal in winter within the Beaufort gyre. This tendency suggests the Arctic deep basin to become even more oligotrophic in the future [*McLaughlin and Carmack*, 2010; *Coupel et al*., 2015], while on the shelves, retreating sea ice can enhance shelf-break upwelling and increase nutrient supply to the euphotic zone [*Carmack and Chapman*, 2003; *McLaughlin and Carmack*, 2010; *Tremblay et al*., 2011]. On the other hand, changes in freshwater pathways near river mouths (i.e., the Mackenzie River), leading to saltier surface waters in some regions, have also been attributed to recent weakening of the on-shelf stratification [*Peralta-Ferriz and Woodgate*, 2015].

2.2. SCMs and Satellite Chl-*a* Estimates

The inability to detect SCM production with ocean color sensors has spurred discussions on the ability of remote sensing algorithms to derive integrated PP in the Arctic from near-surface Chl-*a* concentrations. *Martin et al*. [2010] found that surface Chl-*a* explained 65% of the integrated Chl-*a* in the euphotic zone, *Arrigo et al*. [2011] suggested that the magnitude of the error resulting from the omission of SCMs in satellite-based PP estimates varies significantly (from 0.2 to 16%) in space over an annual cycle, while *Hill et al*. [2013] suggested a constant PP underestimation of 75% throughout the summer over the entire Arctic ocean. Model studies suggest the SCM accounts for 65–90% of the total annual PP in the stratified waters of the Beaufort Sea [*Martin et al*., 2013] and for about 46% of total Arctic PP (68% if areas significantly influenced by Atlantic or Pacific inflow are excluded) [*Popova et al*., 2010]. *Ardyna et al*. [2013] evaluated the issue in more detail and found that vertical variations in Chl-*a* have limited impact on the annual depth-integrated PP. They indicate that small overestimates in areas with shallow SCMs are somehow compensated for by underestimates found when SCMs are deep. Seasonally, however, deep SCMs can have a substantial impact on depth-integrated PP estimates, particularly in highly stratified and oligotrophic conditions, i.e., in the post bloom state in the Arctic Ocean.

Satellite-based productivity algorithms calculate PP at all depths based on a preset vertical Chl-*a* profile. *Martin et al*. [2010] cautioned that applying general regressions to determine integrated Chl-*a* from surface values developed for lower latitudes [e.g., *Morel and Berthon*, 1989; *Uitz et al*., 2006] can either overestimate Chl-*a* inventories (e.g., at neritic stations) or underestimate them (e.g., in clear, stratified waters with a pronounced SCM). *Ardyna et al*. [2013] confirm that these approaches are not applicable in the Arctic Ocean and suggest the most likely reasons are the exposure of phytoplankton communities to pronounced seasonality associated with light, sea ice, and nutrient availability and the salinity-driven stratification in several Arctic Ocean regions. They propose a novel empirical parameterization with a vertical Chl-*a* distribution specifically tuned to the Arctic Ocean and suggest that regional and seasonal regimes are best addressed with specific submodels.

2.3. Previous Model Studies

Vancoppenolle et al. [2013] and *Popova et al*. [2012] evaluated global ESMs and higher-resolution ocean models (referred to as HROMs), respectively, with respect to their representation of PP in the models. They found reasonable agreement with satellite-derived PP for the recent past, but pointed out the disagreement among both higher-resolution Arctic models and global ESMs with respect to nutrient availability and which factor, light or nutrients, controls present-day and future Arctic productivity. *Popova et al*. [2010] suggest that the variability in Arctic PP can be explained by the maximum penetration of winter mixing, which determines the amount of nutrients available for summer production, and short wave

radiation at the ocean surface which determines light availability. The two processes together could explain more than 80% of the spatial variability in PP. In the western Arctic, the MLD is dominated by haline stratification [e.g., *Peralta-Ferriz and Woodgate*, 2015] and the response to ice retreat in a future climate is not straightforward: Ice retreat both enhances stratification due to increased meltwater and decreases stratification due to enhanced momentum flux acting on the upper ocean. In the Canada Basin, stratification is further strengthened due to freshwater accumulation via strong surface Ekman convergence [*Proshutinsky et al*., 2002; *Jackson et al*., 2011].

Popova et al. [2010] note that main departures to the light and mixed-layer relationship with PP occur in regions that are affected by horizontal advection of nutrients (e.g., the southern Chukchi Sea). Model results by *Popova et al*. [2013] indicate significant nutrient contributions to the subsurface layers of the central Arctic Ocean from nutrient-rich Pacific and Atlantic waters on time scales less than 15–20 years (nutrients to the Canada Basin from the Bering Strait are supplied on a time scale of 5–7 years) and from shelves on time scales of 5 years. This shelf transport sustains up to 20% of the total PP in the Arctic Ocean, but can regionally be much higher, e.g., 50–60% in the eastern Makarov and Amundsen Basins and the central Canada Basin. Their study emphasizes the importance of accurate modeling of Arctic Ocean circulation patterns to adequately represent biological production. A model intercomparison evaluating the vertical structure of PP, Chl-*a*, or NO_3 has not been performed yet.

3. Materials and Methods

3.1. Model Descriptions

Analyzed in this study are simulations for the future 2006–2085 period using the representative concentration pathway RCP 8.5 (reaching a >1370 ppm atmospheric CO_2^- equivalent in 2100) [*Moss et al*., 2010]. Model data were regridded to a uniform $2^\circ \times 2^\circ$ grid for all ESMs and $1^\circ \times 1^\circ$ grid for the HROMs via distance-weighted average remapping of the four nearest neighbor values using Climate Data Operators (http://www.mad.zmaw.de/Pingo/post/post.cdo.home.html).

ESM data averaging for a representative area of the Canada Basin, 73°N–79°N and 130°W–150°W (indicated in Figure 1), were done from the regridded data files. HROM data have been averaged on their original grids and provided by participating institutions. For this analysis, model variables are shown as time series or means for the two bidecadal time periods 2006–2025 and 2066–2085. All data have been interpolated to a standard vertical grid with 10 m intervals down to 105 and 25 m intervals down to 350 m.

The ESMs included in this study are the Canadian ESM version 2.0 (CanESM2) Geophysical Fluid Dynamics Laboratory ESM (GFDL-ESM2M), Met Office Hadley Center ESM (HadGEM2-ES), Institut Pierre Simon Laplace low-resolution ESM (IPSL-CM5A-LR), Japan Agency for Marine-Earth Science and Technology ESM (MIROC-ESM), and Max Planck Institute for Meteorology low-resolution ESM (MPI-ESM-LR). The required biogeochemistry fields (Chl-*a* and NO_3), as well as fields of sea ice cover, temperature, and salinity, were accessed via the CMIP5 data portal (http://cmip-pcmdi.llnl.gov/cmip5/data_portal.html). The study builds on the analysis of Arctic Ocean acidification described in *Steiner et al*. [2014] where the six ESMs provided a good representation of the available ESMs. A summary of the models is provided in Table 1. The marine ecosystem is represented either via single representations of nutrient (N), phytoplankton (P), zooplankton (Z), and detritus (D) groups (NPZD, for CanESM2 and MIROC-ESM); via enhanced representations including 2–3 limiting nutrients and one or two phytoplankton groups (MPI-ESM, HadGEM2-ES); or via multiple representatives of all groups, adding up to >20 tracers (GFDL-ESM2M, IPSL-CM5A).

In addition to those coarse resolution global models we include three HROMs, the Los Alamos National Lab-University of Alaska Fairbanks (LANL-UAF) model, the Nucleus for European Modeling of the Ocean-Model of Ecosystem Dynamics, nutrient Utilization, Sequestration and Acidification (NEMO-MEDUSA) model and the North Atlantic Arctic-Canadian Model for Ocean Carbon (NAA-CMOC) model (Table 1). LANL-UAF is a more recent version of the LANL model [*Popova et al*., 2012; *Jin et al*., 2012a]. It has been modified to improve modeled MLD in the Arctic Basin [*Jin et al*., 2012b]. The model is global with high resolution in the Arctic. It consists of linked pelagic and sea ice algal components [*Jin et al*., 2012a] incorporated into a global version of the Parallel Ocean Program-Los Alamos sea ice model POP-CICE. The pelagic component is a medium-complexity model [*Moore et al*., 2004], with multiple nutrients, three types of phytoplankton as well as explicit carbon, iron, and Chl-*a* pools for each

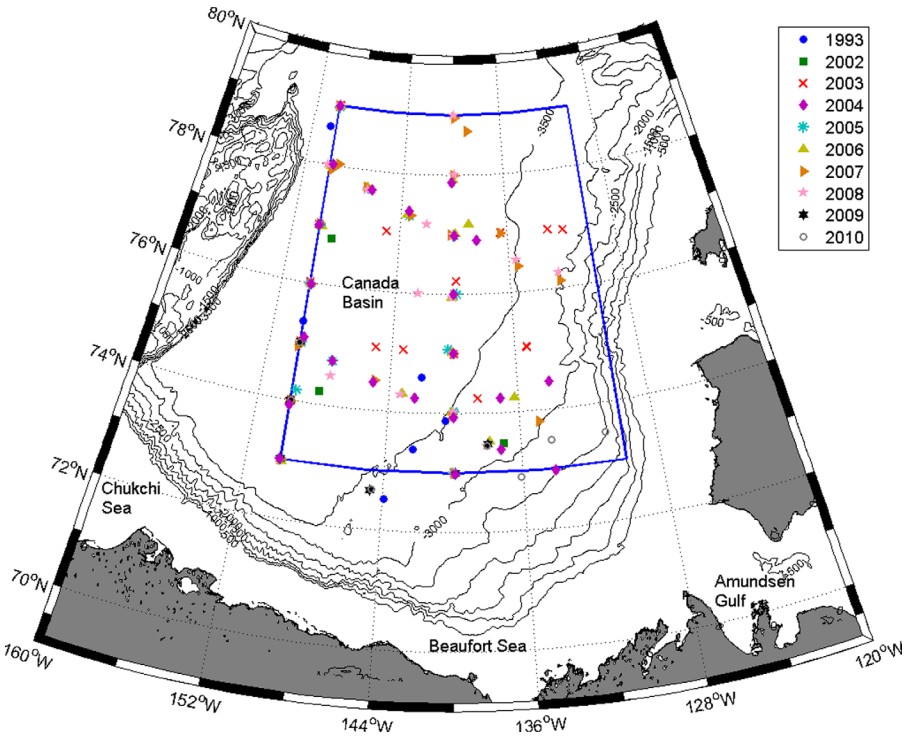

Figure 1. Section of the western Arctic including the Canada Basin Beaufort Sea area. Colored symbols show locations of the observed profiles included in Figure 3 by year. The blue frame indicates the model domain used for the basin averages.

phytoplankton group, and the herbivorous zooplankton pool. The ice algal component represents colonies in a 3 cm layer at the bottom of each sea ice thickness category, coupled to the pelagic model through nutrient and biotic fluxes [*Jin et al*., 2006, 2007; *Deal et al*., 2011]. Initial conditions for chemical variables (NO_3, Si) are from the gridded World Ocean Atlas (WOA2005) and for other constituents from a global model simulation by *Moore et al*. [2004]. LANL-UAF has been forced with output from the GFDL-ESM2M for RCP8.5.

The NEMO-MEDUSA model is a high-resolution global ocean biogeochemical model. The underlying physical model is NEMO [*Madec*, 2008] coupled with a sea ice model, Louvain-la-Neuve Ice Model version 2 (LIM2) [*Timmermann et al*., 2005]. MEDUSA-2.0 is an intermediate complexity ecosystem model that divides the plankton community into small and large portions, and which resolves the elemental cycles of nitrogen, silicon, Fe, C, alkalinity, and oxygen with 15 state variables in total [*Yool et al*., 2013b]. NEMO-MEDUSA is forced with output from HadGEM2-ES for RCP8.5. Temperature and salinity fields are initialized using output from HadGEM2-ES valid for the same time as the forcing. To prevent excessive drift, sea surface salinities are relaxed toward those derived from HadGEM2-ES. Biogeochemical variables are initialized with data from World Ocean Atlas 2009 and Global Ocean Data Analysis Project (GLODAP) climatologies [*Yool et al*., 2013a; *Popova et al*., 2014].

The NAA-CMOC model is a regional model for the Arctic based on NEMO-LIM2 in the configuration by *Hu and Myers* [2013, 2014] with the Canadian Model of Ocean Carbon (CMOC) ecosystem component [*Zahariev et al*., 2008; *Christian et al*., 2010] which is the same as in CanESM2, but updated to include oxygen. NAA-CMOC is forced with output from the 22 km resolution Canadian Regional Climate Model version 4 (CanRCM4) [*Scinocca et al*., 2016] covering the Coordinated Regional Climate Downscaling Experiment (CORDEX Arctic) domain, merged with CanESM2 data in the small area where CanRCM4 does not fully cover the NAA domain. CanRCM4 is forced with CanESM2 output on its horizontal boundaries. NAA-CMOC has only been run with climatological mean forcing for the time periods of 2006–2025 and 2066–2085 for 10 years each, with both time periods initialized with CanESM2 output from the respective RCP8.5 run.

3.2. Calculation of the SCM and Other Indicator Variables

While not all papers discussing observed SCMs define how the SCM has been calculated, most analyses identify the SCM depth as the depth where fluorescence is highest [e.g., *McLaughlin and Carmack*, 2010; *Jackson et al*., 2010a; *Martin et al*., 2010]. *Martin et al*. [2013] also define an upper limit for SCMs, i.e., the depth where a positive gradient of 0.01 μg Chl-*a* L^{-1} m^{-1} is attained relative to the surface Chl-*a* and where Chl-*a* was equal to or greater than 0.11 μg L^{-1}. Below that depth, the SCM was defined as the depth where Chl-*a* was at maximum.

For the models, Chl-*a* values are interpolated to the standard depths from each model, the depth with the highest Chl-*a* value is flagged and used for the SCM depth. This measure works well for the annual and seasonal means of the study area (Figure 1).

Chl-*a* in the models is calculated via either constant or varying Chl-*a*:C or Chl-*a*:N ratios (Table 1). Constant Chl-*a*:C ratios vary from 0.017 mg Chl-*a* mg C^{-1} (MPI-ESM-LR) to 0.025 mg Chl-*a* mg C^{-1} (HadGEM2-ES). Varying Chl-*a*:C or Chl-*a*:N ratios are predicted based on the external concentrations of the limiting nutrients (IPSL-CM5A-LR) or take into account photoacclimation by including changes in the ratio of energy assimilated to energy absorbed [*Geider et al*., 1996, 1997], using maximum Chl-*a*:C ratios between 0.03 and 0.05 mg Chl-*a* mg C^{-1}. The CMIP5 database does not provide monthly resolved ESM output for Chl-*a*. However, for the Canada Basin, the pattern of the vertical Chl-*a* distribution is well represented by the annual mean, even though the magnitude of the annually averaged Chl-*a* concentration is lower than a summer only average. This has been tested with CanESM2 and examples are shown for the HROMs (Figures 5, 8h and 8i).

In addition to the SCM, several indicator variables have been chosen to help understand the observed and simulated changes: NO_3 at the SCM, the depth of the 33.1 psu isohaline (core of the Pacific Winter Water) [*McLaughlin and Carmack*, 2010], mean salinity in the top 40 m, and freshwater content (FWC). FWC, integrated over the upper 500 m (in units of m), is defined as:

$$FWC = \int_0^{350m} \frac{(S_r - S)}{S_r} dz\,, \tag{1}$$

with salinity S referenced to $S_r = 34.8$ [e.g., *Steiner et al*., 2004].

3.3. Observations

Observed profiles of salinity, temperature, fluorescence, and NO_3 were collected from icebreakers during July, August, and September 1993–2010 under collaboration of researchers from Fisheries and Oceans Canada, the Japan Agency for Marine-Earth Science and Technology, and the Woods Hole Oceanographic Institution (http://www.whoi.edu/beaufortgyre). Salinity, temperature, and pressure data were collected with a SeaBird 911-Plus CTD from 2002 to 2010 (details in *McLaughlin et al*. [2008]) and with a FSI CTD ICTD in 1993 [*Macdonald et al*., 1995]. Fluorometer data were collected with a Seapoint fluorometer from 2002 to 2010 and calibrated with Chl-*a* values measured from bottle samples. Nitrate data were collected from bottle samples. Locations of the individual profiles are indicated in Figure 1 and averaged over the area indicated by the black line. Observed average profiles were separated into two time periods, with the second period starting with the initial year of the RCP8.5 projection simulations. Data from 67 profiles contributed to the 1993–2005 profiles and 88 profiles to the 2006–2010 profiles. From the observed data, density and Chl-*a* profiles have been derived and are provided together with the 95% confidence interval. Due to poor vertical resolution in NO_3 profiles a centered 9 m running mean has been calculated for each individual profile and again for the average profile for each time period. Averaged salinity, temperature, fluorescence, and NO_3 data used to create the plots are provided in the supporting information (supporting information Table S1).

4. Results

4.1. The Recent Past in the Canada Basin

Comparisons of climate projection runs with actual years of observations need to be viewed with caution. Climate models tend to create their own internal variability which does not necessarily correspond with the interannual and decadal variability in the observations. Based on these constraints and the given sparsity of

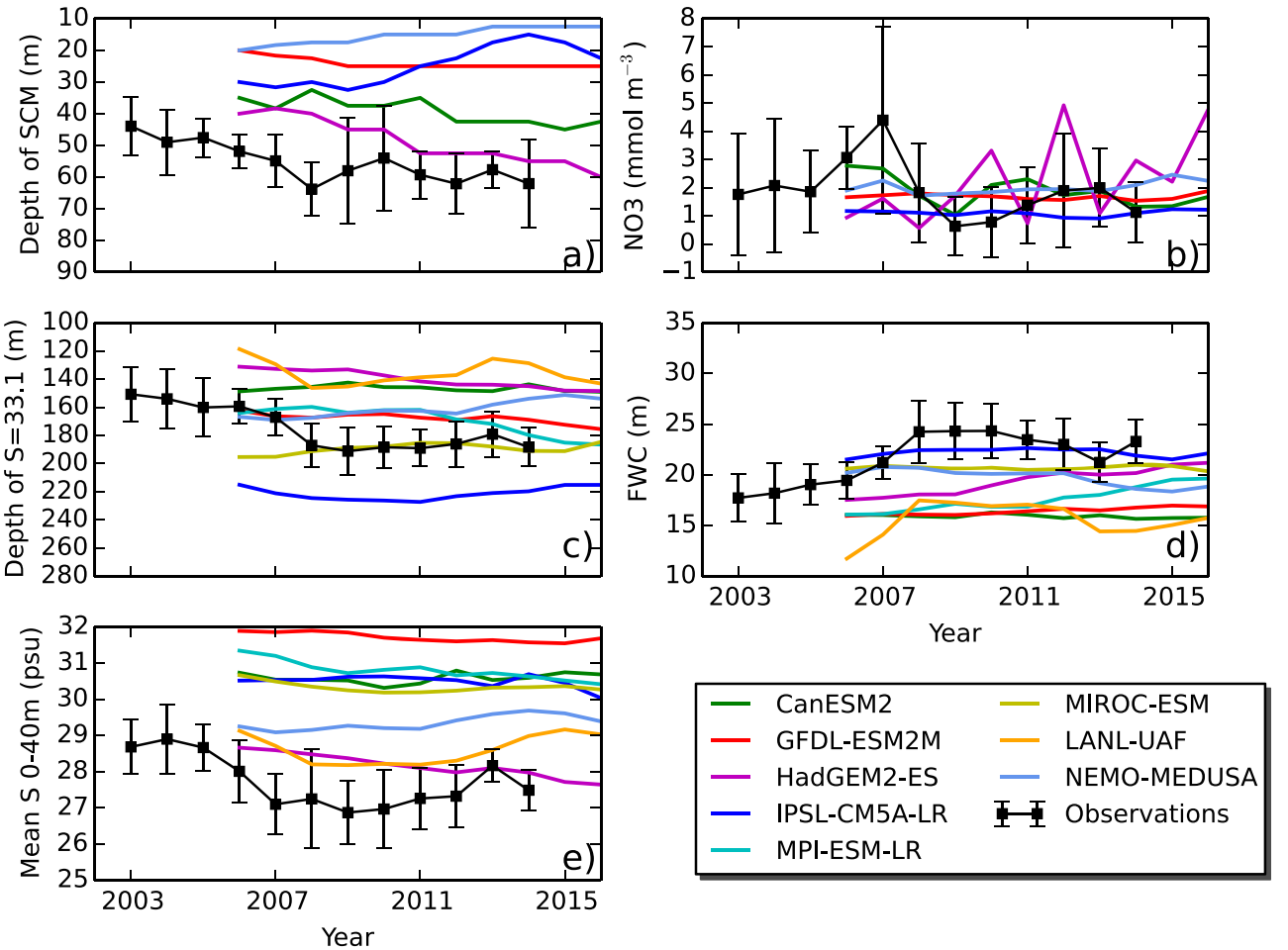

Figure 2. Observed and simulated (a) depth (m) of the SCM, (b) NO_3 (mmol m^3) at the SCM depth, (c) depth (m) of the 33.1 isohaline, (d) freshwater content (m) (referred to a salinity of 34.8 psu), and (e) mean salinity in the top 40 m for the years 2003–2014 (as available) and for the following models: CanESM2, GFDL-ESM2M, HadGEM2-ES, IPSL-CM5A-LR, NEMO-MEDUSA, and observations. Observations are extensions from basin-averaged data presented in *McLaughlin and Carmack* [2010], *McLaughlin et al.* [2011], and S. Zimmermann (Institute of Ocean Sciences, Sidney, personal communication, 2015). Basin-averaged calculations include data from stations with bottom depths greater than 1600 m and located 72.5°N to 78.2°N and 139°W to 153.5°W.

biological observations in the Arctic (e.g., review by *Steiner et al.* [2015]), basin-scale averaging and to a certain extent temporal averaging is the most reasonable way to evaluate the performance of biogeochemical modules in climate models at this point in time.

4.1.1. Time Series of the SCM and Indicator Variables

To evaluate the models' initial conditions and general tendency over the first decade of the projection runs, Figure 2 shows time series of basin-averaged (Figure 1) model results and observations. Some models are unable to simulate a SCM (see discussion below) or have no available time series information (NAA-CMOC) and have been excluded from Figures 2a and 2b. Observations shown are extensions of time series presented in *McLaughlin and Carmack* [2010] and *McLaughlin et al.* [2011]. For 2003–2010, *McLaughlin and Carmack* [2010] show a freshening of the winter mixed layer by about 2 psu and a deepening of the 30 and 33.1 psu isohalines by about 40 m. *McLaughlin and Carmack* [2010] indicate the 30 psu isohaline as the depth of the winter halocline (which separates the wintertime mixed layer from underlying Pacific Summer Water) and the 33.1 psu isohaline as the core of the Pacific Winter Water, respectively. This tendency seems to have leveled off in recent years where values remained constant or show a slightly reverse trend.

For this short time period (2006–2015), an increase in freshwater content is not obvious in the models, although a slight deepening (less than 20 m) in the 33.1 psu isohaline can be seen in some models as well as a slight reduction (less than 1 psu) in the top 40 m mean salinity (Figures 2c–2e). Differences among the models are likely linked to the timing of sea ice retreat simulated in the models: The IPSL-CM5A-LR and

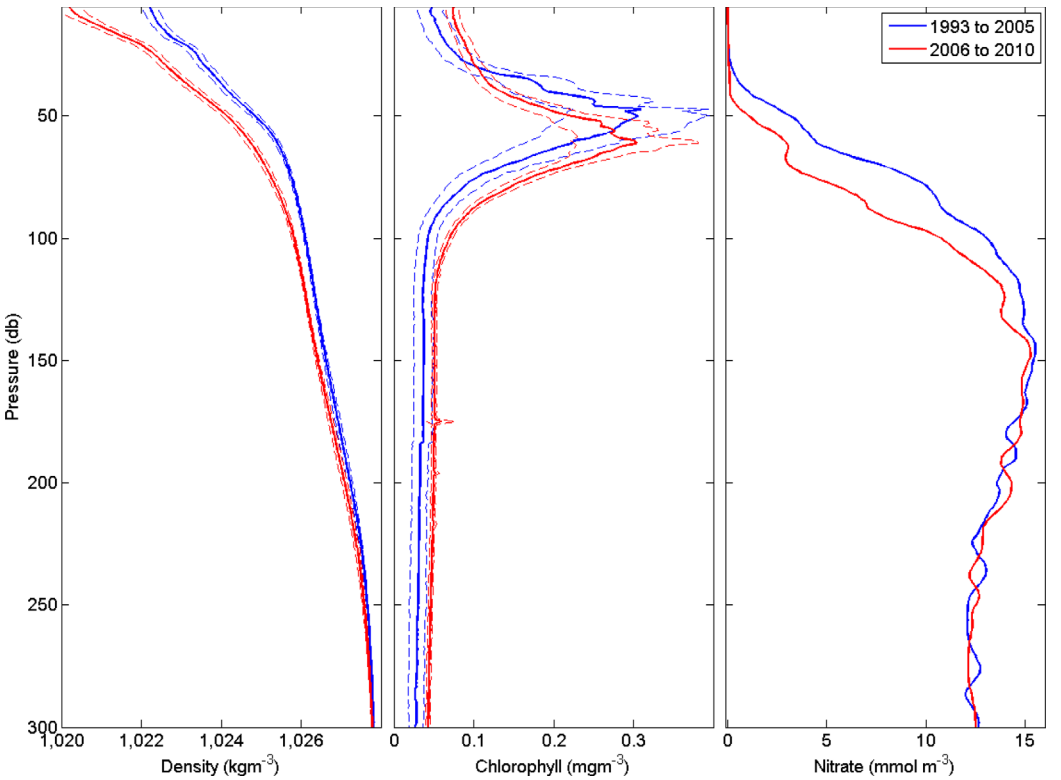

Figure 3. Observed average profiles including data from 67 profiles for 1993–2005 and 88 profiles for 2006–2010 collected in July, August, and September (majority in August) under the U.S./Canada BGOS/JOIS projects (http://www.whoi.edu/beaufortgyre). Dashed lines indicate the 95% confidence interval. (a) Density, calculated from measured temperature and salinities, (b) Chl-*a*, from measured and calibrated fluorescence, and (c) NO_3. Due to poor vertical resolution in nitrate profiles, a centered 9 m running mean has been calculated for each individual profile and again for the average profile for each time period. Locations of the individual profiles are indicated in Figure 1. Averaged salinity, temperature, fluorescence, and nitrate data used to create the plots are provided in supporting information Table S1.

GFDL-ESM2M models show a later loss of summer sea ice in the Canada Basin, while CanESM2 and HadGEM2-ES show an earlier summer ice loss [*Steiner et al*., 2014, Figure 4d]. Earlier ice loss is also simulated for NEMO-MEDUSA (not shown).

Only some of the models show a deepening in the SCM for this short time period and the modeled depth of the SCM is generally shallower than the observed one (Figure 2a). Modeled SCMs start off between 20 and 40 m in 2005 and are simulated to deepen by 5–20 m over the 10 year time period, while in the observations the SCM deepens from 45 to 65 m. The simulated NO_3 concentration at the SCM is generally in good correspondence with the observations and some models show similar variability to the observations (Figure 2b, CanESM2). Compared to other models the HadGEM model (magenta line) shows much higher interannual variability.

4.1.2. Vertical Profiles

Figure 3 shows basin averaged profiles for observed density, Chl-*a* and NO_3 for 1993–2005 (blue lines) and 2006–2010 (red lines). The observations indicate a decrease in density due to freshening in the upper ocean waters traceable to at least 150 m depth, about a 10 m deepening of the SCM with very little change in magnitude, and a reduction in NO_3 content also traceable to about 150 m depth. The first plot in Figures 4–7 shows modeled profiles of Chl-*a* (annual mean and summer), density, and NO_3 for the time period 2006–2025 for all the models together with the observed profiles from summer 2006–2010.

The observed depth structure for Chl-*a* (identifiable SCM below 50 m) is most closely represented by the CanESM2, NAA-CMOC, and to a certain extent HadGEM2-ES models (Figure 4a, note that the annual mean Chl-*a* concentration is lower than the summer mean). At the same time NAA-CMOC shows too low Chl-*a* concentrations at the surface and a similar but even deeper SCM feature than its driving model CanESM2.

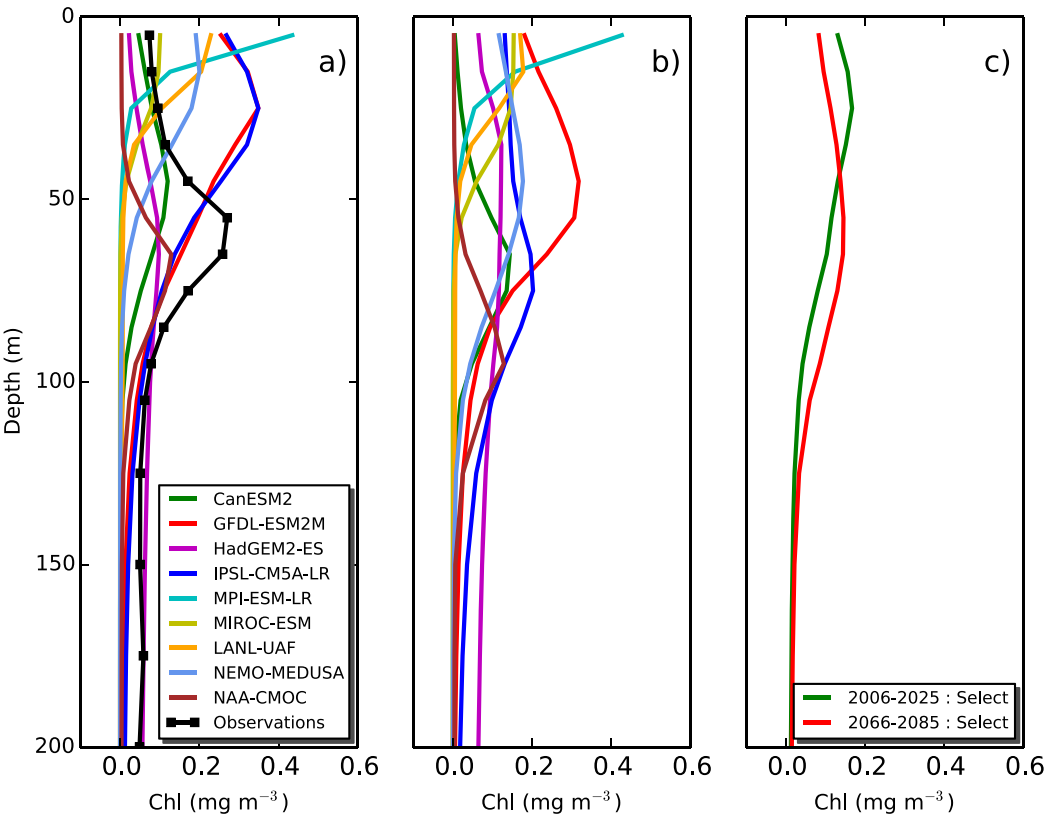

Figure 4. Simulated bidecadal averages of the annual mean vertical Chl-*a* profiles (mg m^{-3}) for the various ESMs and HROMs averaged over the area 73°N–79°N and 130°W–150°W. (a) 2006–2025, (b) 2066–2085. (c) The multimodel mean for both time periods excluding the MPI-ESM-LR, MIROC-ESM, and LANL-UAF models which do not show a SCM. The observed profile for 2006–2010 (summer) from Figure 3 has been overplotted in Figure 4a.

The GFDL-ESM2M, IPSL-CM5A-LR, and NEMO-MEDUSA SCMs are too shallow and too high (annual mean is higher than summer observations, see also Figure 2a). MPI-ESM-LR and LANL-UAF show high surface Chl-*a* with no SCM. MIROC-ESM has no SCM and somewhat lower surface Chl-*a*. The intercomparison in Figure 2 also illustrates that a good representation of surface Chl-*a* does not necessarily translate into an accurately modeled vertical profile. The July/August profiles (Figure 5, HROMs only) confirm the indicated differences in vertical structure, but also show that simulated Chl-*a* concentrations at the SCM are reasonable. Figure 5 also shows the vertical profile of PP (dotted lines, scaled to fit the Chl-*a* panel) for the HROMs. While the Chl-*a* and PP profiles are not directly interchangeable, they show the same characteristic features for the individual models and indicate the same differences among the models. If a SCM is simulated, it shows up more prominently in the Chl-*a* profile than in the PP profile.

The simulated annual mean density does not reflect the steep density gradient observed at the surface in the summer months (Figure 6), which is, to a certain extent, a result of the annual averaging. The models show clear intermodel differences in the top 100 m, which reflect differences in salinity potentially caused by different rates of sea ice retreat, but also indicative of differences in the model's strength of the Beaufort Gyre circulation and consequent accumulation of freshwater in the Canada Basin.

The NO_3 profiles (Figure 7a) reflect the large intermodel differences discussed above. The HadGEM2-ES model is the only one with a very similar profile to the observation, all others seem to smoothen the NO_3 gradient between near-surface ($<$50 m) and deeper layers ($>$100 m), causing too low values at depth. Exceptions are the MPI-ESM-LR and LANL-UAF models, which are too high at the surface. (Note that near-surface annual means are expected to be somewhat higher than the summer values.)

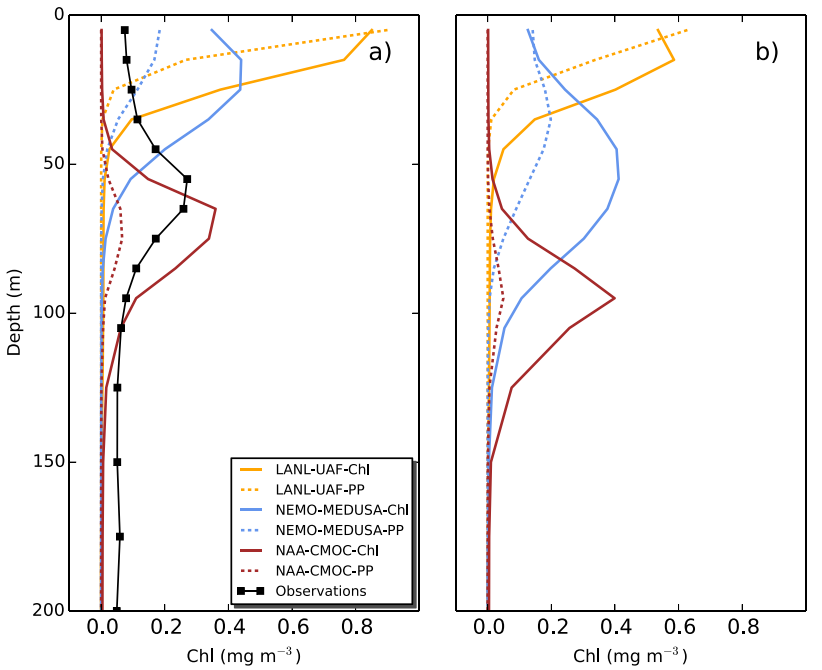

Figure 5. Simulated bidecadal averages of the July/August mean Chl-*a* profiles in mg m^{-3} (solid lines) for the three HROMs and observations averaged over the area 73°N–79°N and 130°W–150°W. Simulated primary production (2.e^{-1} mg C m^{-3} d^{-1}) scaled to fit the Chl-*a* figure has been added for intercomparison (dotted lines). (a) 2006–2025, (b) 2066–2085. The observed profile for 2006–2010 (summer) from Figure 3 has been overplotted in Figure 5a (black line).

4.2. Projections in the Canada Basin

4.2.1. Time Series of the SCM and Indicator Variables

Figure 8 shows the time series (2006–2085) for the basin-averaged annual mean vertical profile of Chl-*a*. The August only time series for NEMO-Medusa is shown in Figure 8i to point out the similarity of the pattern to the annual mean (Figure 8h). Respective time series for NO_3 and density are shown in Figures 9 and 10. Time series for temperature and salinity are added as supporting information Figures S1 and S2.

The evolution of the vertical Chl-*a* profile shows large differences among the models (Figure 8), both in terms of structure and magnitude. Two of the ESMs and one of the HROMs do not represent a SCM at all (Figures 8e, f, g). As indicated in earlier studies [*Popova et al*., 2010, 2012; *Vancoppenolle et al*., 2013], the nutrient supply is likely the major cause. The MPI-ESM-LR and LANL-UAF models have too much NO_3 (Figures 9e and 9g), and hence no surface NO_3 limitation suppressing the production. The MIROC-ESM shows low nitrate throughout the water column (Figure 9f) but still supports surface growth throughout the time period. This suggests that the ecosystem model parameterization might also contribute to the lacking SCM. Both models with too much NO_3 show a decline in surface nutrients over the projected time period, but only so much as to decrease associated growth in surface waters, not enough to initiate subsurface growth. All other models show a continuous deepening of the SCM in the future as suggested by recent observations [*McLaughlin and Carmack*, 2010; *McLaughlin et al*., 2011; *Jackson et al*., 2010b], some models starting with a surface Chl-*a* maximum or shallow SCM, while others already have an established deep SCM in 2006 (CanESM2, HadGEM2-ES). Overplotted in Figures 8–10 are the 30 and 33.1 psu isohalines, indicating the link of both SCM and nutrient distribution to the salinity stratification. The 33.1 psu isohaline, which *McLaughlin and Carmack* [2010] link with the nutrient bearing PWW, is consistently far below the SCM and indicates depths with high NO_3 (mostly around 15 mmol m^{-3}), unless deep NO_3 is simulated very low in the model. For some models, this isohaline does in fact indicate a high nutrient core (HadGEM2-ES, MPI-ESM-LR, and NEMO-MEDUSA). The 30 psu isohaline, which *McLaughlin and Carmack* [2010] identify as the winter halocline, indicates continuous deepening for most of the time period in all models, but GFDL-ESM2M which is too salty (>30 psu throughout). If a deepening of the SCM is represented, it shows some correlation to the 30 psu isohaline, with the SCM being either just below, just above or centered on the isohaline.

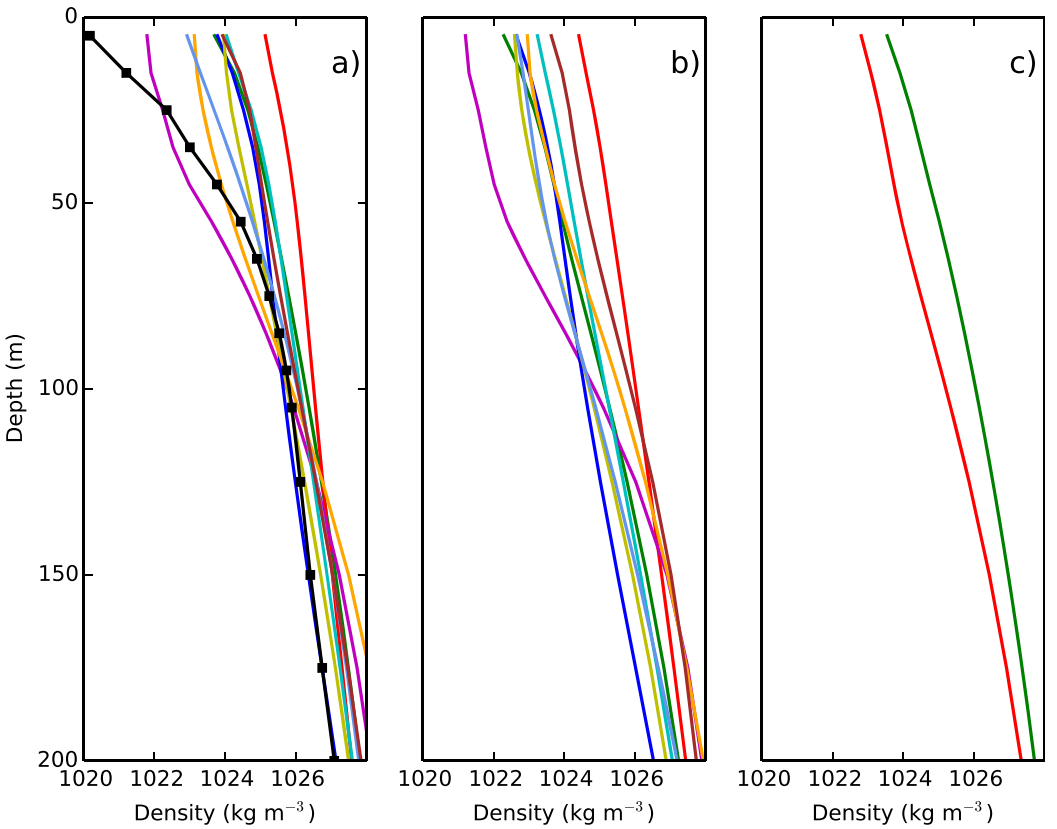

Figure 6. Simulated bidecadal averages of the annual mean vertical density profiles (kg m^{-3}) for the various ESMs and HROMs averaged over the area 73°N–79°N and 130°W–150°W. (a) 2006–2025, (b) 2066–2085. (c) The multimodel mean for both time periods, excluding the MPI-ESM-LR, MIROC-ESM, and LANL-UAF models which do not show a SCM. The observed profile for 2006–2010 (summer) from Figure 3 has been overplotted in Figure 6a. Figure legend as in Figure 4.

Figure 11a shows the depth of the SCM (only models representing a SCM). The SCM as indicated in the annual mean varies within a range of 50 m among the models. Both representations (Figures 8 and 11a) show the SCM depth to level off sometime between about 2050 and 2065, which is when the models reach a state of ice-free summers in the Canada Basin [*Steiner et al*., 2014]. The HadGEM-ES shows an uplift in the SCM at the end of the time series. Trends are 0.08 m yr^{-1} for HadGEM-ES and between 0.42 and 0.72 m yr^{-1} for the other models (Table 2). The HadGEM-ES trend falls into the same range as the other models if the last decade is excluded.

4.2.2. Vertical Profiles of Chl-a

Annual mean Chl-*a* profiles for the same region, averaged over current and future bidecades, 2006–2025 and 2066–2085, are presented in Figure 4. The models with a representative SCM show a deepening over time, however the simulated change is quite variable among the models. The GFDL-ESM2M and IPSL-CM5A-LR models show a very similar structure for the current time period, but in the future IPSL-CM5A-LR transitions to a deeper, but weaker SCM than GFDL-ESM2M. HadGEM-ES, which did show an initial deepening in the SCM (Figure 8), shows a broadened maximum at a lower depth by 2066–2085. For the HROMs, LANL-UAF does not show a SCM in either time periods and the NEMO-MEDUSA and NAA-models show a SCM deepening of 25–30 m. Chl-*a* in NAA-CMOC is generally low and the SCM pronounced. The multimodel mean (Figure 4c) shows a deepening of about 40 m for the SCM with very little change in magnitude, if the three models which do not represent a SCM are excluded. The July/August profiles for the HROMs NEMO-Medusa and NAA-CMOC (Figure 5) also indicate a deepening of the SCM (solid lines) as well as a deepening in the subsurface PP (dotted lines) maximum. For NEMO-Medusa, the subsurface maximum becomes more prominent in the future. LANL-UAF simulates reduced surface production in the future.

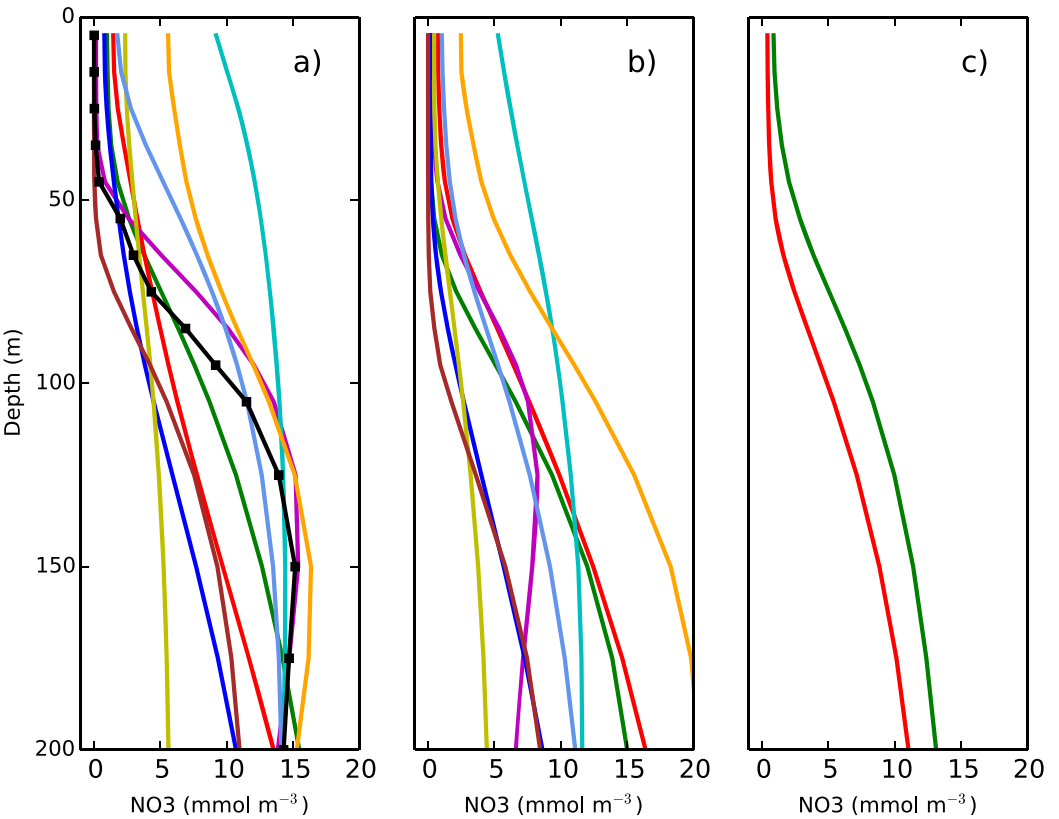

Figure 7. Simulated bidecadal averages of the annual mean vertical NO_3 profiles (mmol m^{-3}) for the various ESMs and HROMs averaged over the area 73°N–79°N and 130°W–150°W. (a) 2006–2025, (b) 2066–2085. (c) The multimodel mean for both time periods, excluding the MPI-ESM-LR, MIROC-ESM, and LANL-UAF models which do not show a SCM. The observed profile for 2006–2010 (summer) from Figure 3 has been overplotted in Figure 7a. Figure legend as in Figure 4.

4.2.3. Density Stratification

All models show a continuous freshening with retreating sea ice (supporting information Figure S1; isohalines in Figure 8). This leads to an accumulation of freshwater (increased FWC) and a deepening of the 33.1 psu isohaline (Figures 11c and 11d). Despite the differences among the models in absolute value and interannual variability, the trend over the 80 years for all salinity and stratification related variables is remarkably similar (Figure 11). For example, for the majority of the models, the depth of the 33.1 psu isohaline deepened by 0.6–0.9 m yr^{-1} and the FWC increased by 0.11–0.13 m yr^{-1} (Table 2). Lower trends were found for GFDL-ESM2M, likely due to slower ice decline [*Steiner et al*., 2014], and for HadGEM2-ES, likely due to a changed pattern in the last two decades. Corresponding trends in decreasing NO_3 were found at a rate of -0.006 mmol m^{-3} yr^{-1}, again with the exception of HadGEM2-ES which shows both a faster NO_3 decline (-0.01 mmol m^{-3} yr^{-1}), and higher variability (Table 2 and Figure 11b). Figure 9 indicates erosion of the NO_3 core from the top and the bottom for HadGEM2-ES, which might cause the high variability.

The isohalines level off once a more stable seasonal sea ice cycle is reached and in some cases the FWC even starts to decrease again. Both the HadGEM2-ESM and Nemo-MEDUSA models show a similar pattern from about 2045 with a slight decrease in FWC after 2050. NEMO-MEDUSA even shows a sudden increase in salinity for all layers after 2080 and an uplift in the 33.1 psu isohaline. This is likely related to a very thin ice cover through winter, causing lower summer melting and enhanced wind mixing, which in turn leads to a loss of stratification. The similarity in the freshwater accumulation for both the NEMO-MEDUSA and HadGEM2-ES models suggests that larger-scale atmospheric circulation patterns are transferred from the forcing large-scale model, driving similar features in both the ESM and the HROM.

Temperatures reflect enhanced surface warming as well as enhanced Atlantic water temperatures. Likely both diffusive and turbulent mixing processes then also warm the intermediate waters (supporting information Figure S1). Figure 10 represents the density evolution for the basin average, indicating a continuous shift to

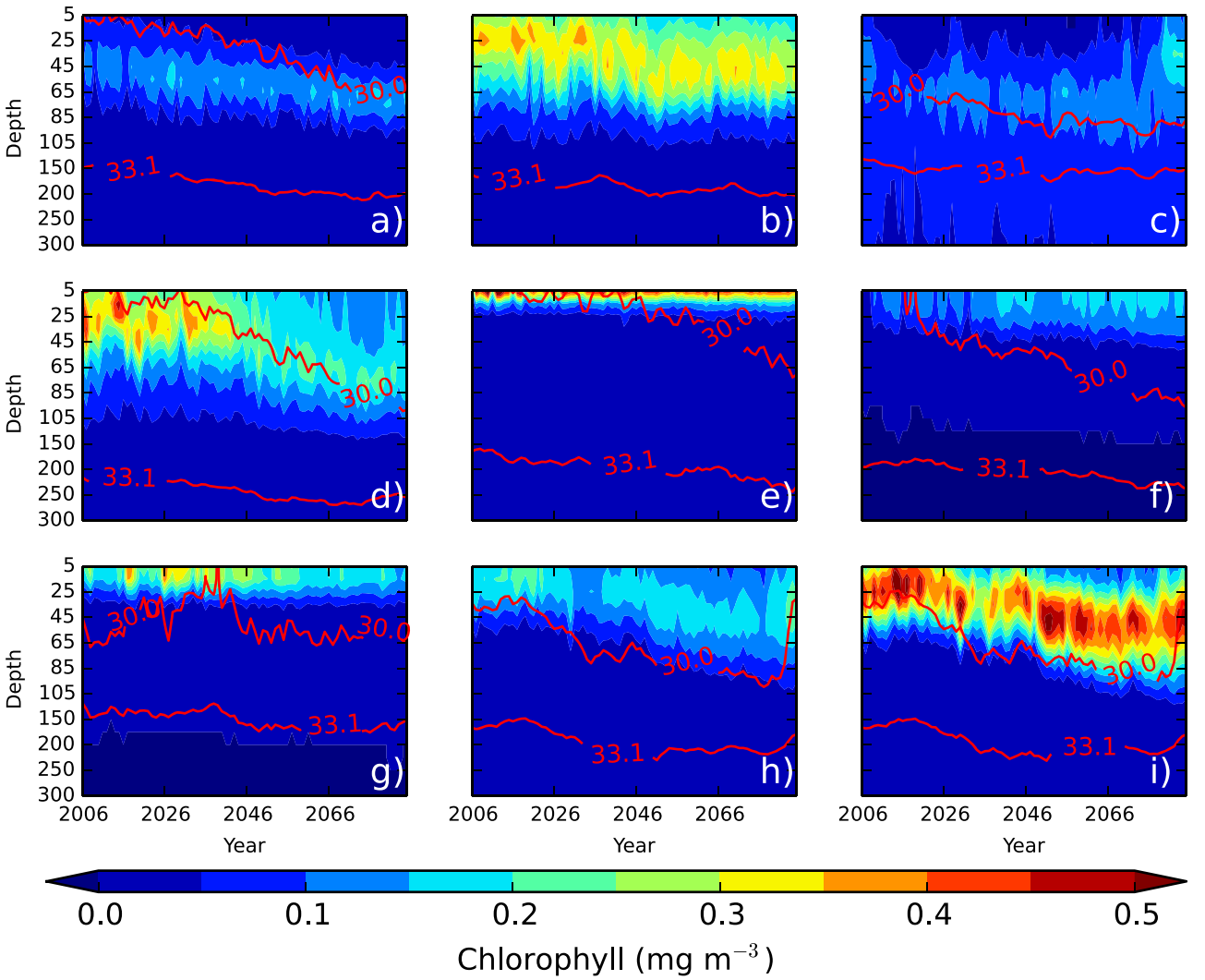

Figure 8. Projected time series of the vertical Chl-*a* distribution (mg Chl-*a* m^{-3}) averaged over the area 73°N–79°N and 130°W–150°W for 2006–2085. (a–h) Annual mean and (i) August mean. (a) CanESM2, (b) GFDL-ESM2M, (c) HadGEM2-ES, (d) IPSL-CM5A-LR, (e) MPI-ESM-LR, (f) MIROC-ESM, (g) LANL-UAF, (h) NEMO-MEDUSA, and (i) NEMO-MEDUSA—August. Overplotted in red are the 30 and 33.1 psu isohalines.

lower-density waters in the upper ocean. Overplotted isohalines (black lines) underline the predominant salinity stratification in the domain. Also overplotted are density changes of 0.1 and 0.3 kg m^{-3} from the surface. *Peralta-Ferriz and Woodgate* [2015] summarize 0.1 kg m^{-3} to best match the heuristic measure of the MLD. Unfortunately in the models, limited vertical resolution tends to cause this jump to occur between layer one and two. In addition, the annual averaging tends to smear out the near-surface stratification features which are seasonally variable. Hence, tracking modeled MLD in the models does not enhance this study.

4.3. Ratio of Surface to Integrated Chl-*a*

To address the question of potential changes in the interpretation of satellite Chl-*a* in a future climate, the ratio of the Chl-*a* surface concentration to the concentration in the upper 200 m has been evaluated. However, defining "surface Chl-*a*" is not straightforward, since satellite sensors detect a signal from the upper few meters of the ocean and this is affected by absorbance of radiation by the precise pattern of Chl-*a* in this region. Here we chose to present a depth of 5 m, which corresponds closely with the surface layer in most models. However, the analysis has also been performed for the top 10 m and results will be included in the discussion. Figures indicating the integrated Chl-*a* concentrations and respective ratios for all models in the past and future are provided in supporting information Figures S3–S5 and a summary for the Canada Basin area is provided in Table 2. While the ratios show significant differences among the models, the changes over time show much less variability (Figure 12, showing 5–200 m integrals). Most

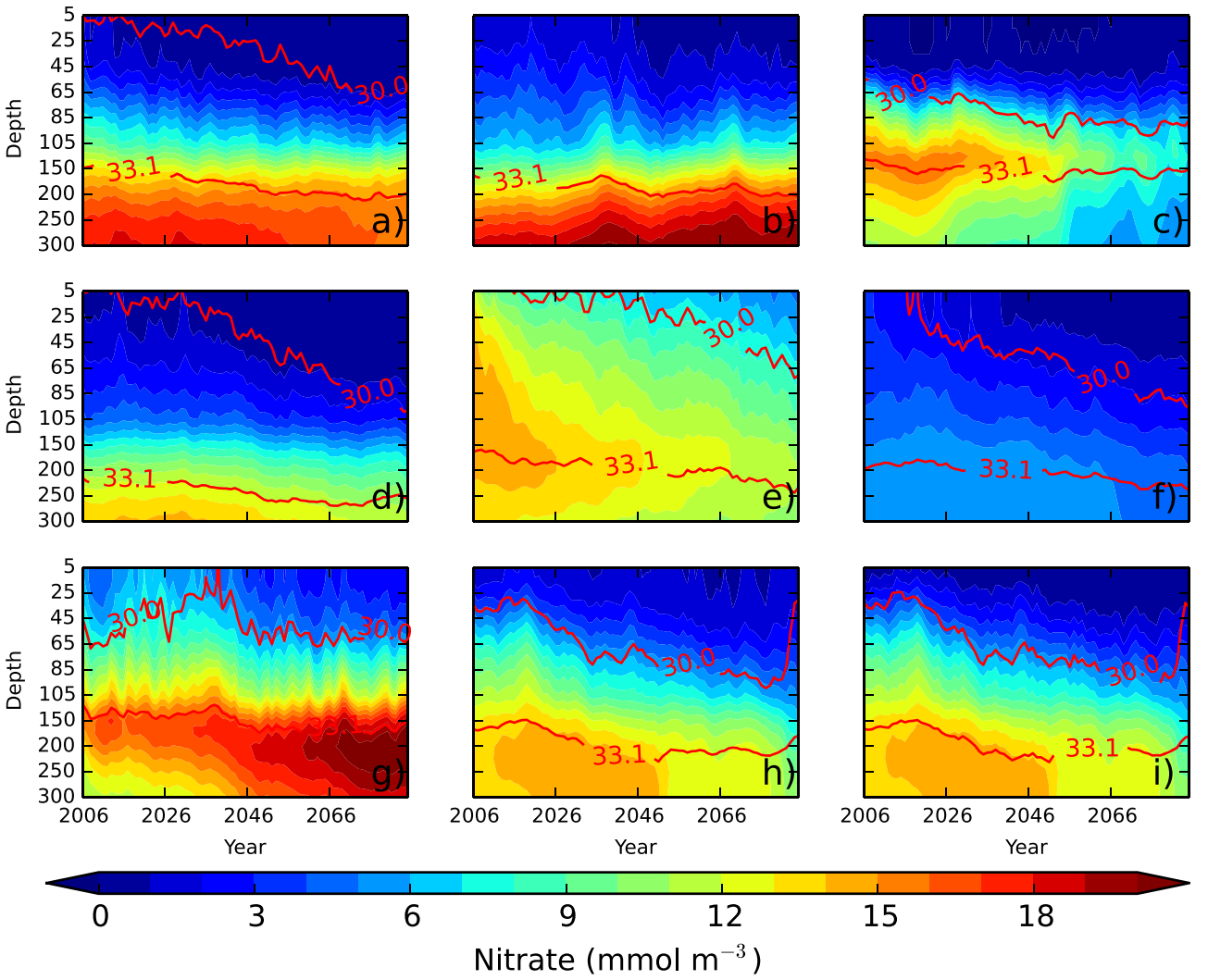

Figure 9. Same as Figure 8 but for NO_3 (mmol m^{-3}).

models show a decline in the ratio for almost all areas of the Arctic, indicating an enhanced contribution of subsurface Chl-*a* production. Lower values or even slight increases and hence increased contributions by surface production are mostly seen on shelf areas and in the eastern Arctic. An exception is the HadGEM-ES model which shows a clear increase in the surface to integrated Chl-*a* ratio in the Canada Basin, which is caused by enhanced near-surface production simulated for that model toward the end of the simulated time period (Figures 4 and 8). The 10–200 m ratios and differences between future and current times show the same pattern with somewhat higher values. NAA-CMOC shows changes close to zero and the color coding in (Figure 12) might be somewhat misleading. A visual comparison of Chl-*a* in the top 5 m and in the upper 200 m for current and future times (supporting information Figures S3 and S4) suggests inconsistent increase or decrease in surface Chl-*a* but a more general increase in the 200 m integrated Chl-*a*, confirming the suggested increase of subsurface production in the future. Averaged over the Canada Basin domain, the results are not as straight forward (Figure 13 and Table 2) since both increases and decreases occur for 5 m (10 m) and 200 m integrations. However, most models show a slight decrease in surface production and a slight increase in integrated production. In all cases, but for the HadGEM-ES model, the increase in subsurface production dominates the change leading to a reduction in the surface to integrated Chl-*a* ratio for all the models. The 10 m integral and the 10–200 m ratios are about twice those for 5 m (Table 2), supporting the suggestion of increased contributions from the SCM. Among the models representing a SCM, largest changes in the surface to integrated Chl-*a* ratio are seen for NEMO-MEDUSA and CanESM2 (Figure 13). Changes in the GFDL-ESM2M and IPSL-CM5A-LR models are very similar to each other with a fairly consistent decline over the full time period. NAA-CMOC has not been run

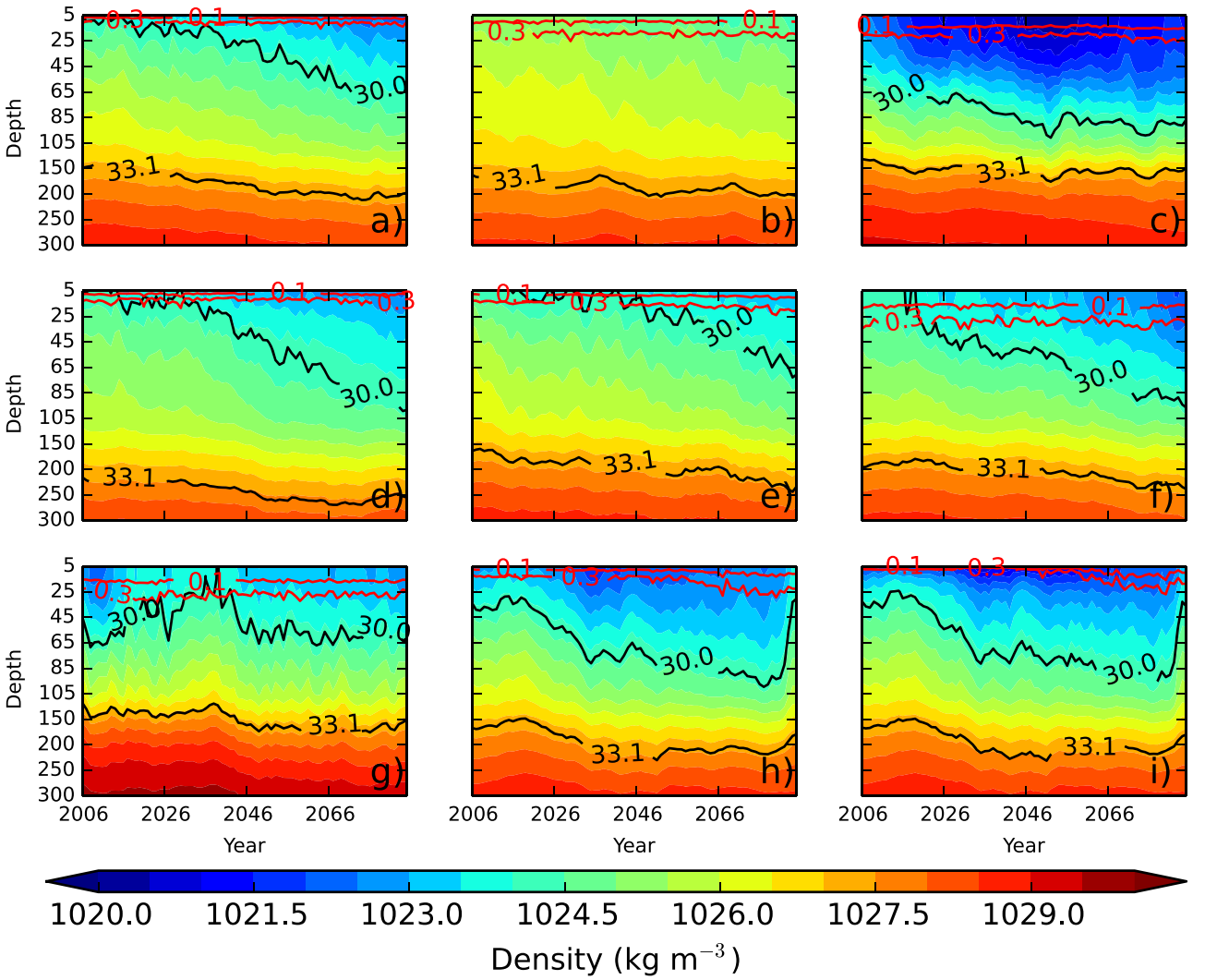

Figure 10. Same as Figure 8 for density (kg m^{-3}). Overplotted in black are the 30 and 33.1 psu isohalines. Red lines indicate density changes of 0.1 and 0.3 kg m^{-3} from the surface.

in time series mode, but bidecadally averaged data support the main tendencies suggested by the other models (Table 2). Models which do not represent a SCM still show a reduced surface to integrated Chl-*a* ratio, with Chl-*a* increases in the surface and deeper layers for the MPI-ESM-LR and MIROC-ESM models and decreases for both in the LANL-UAF model.

5. Discussion

5.1. General Comments

Based on the sparsity of biogeochemical observations in the Arctic and the inability of climate models to accurately represent observed interannual variability, basin-scale and temporal averaged data have been used to evaluate biological model performance. The presented results provide some indication on the projected future changes of subsurface and surface Chl-*a* production, but they need to be viewed with caution and should be revisited once nutrient databases are improved and Arctic ecosystem as well as physical models can be better validated. *Popova et al.* [2012] suggested that as long as one of the two limiting factors, light or nutrients, is reproduced correctly, simulated PP in the recent past is close to the one observed. However, they point out that a potential decoupling of sea ice and nutrient limitation in the future might reduce the predictive capabilities of the models, unless the processes affecting the nutrient supply mechanisms are better represented in the models, particularly vertical mixing.

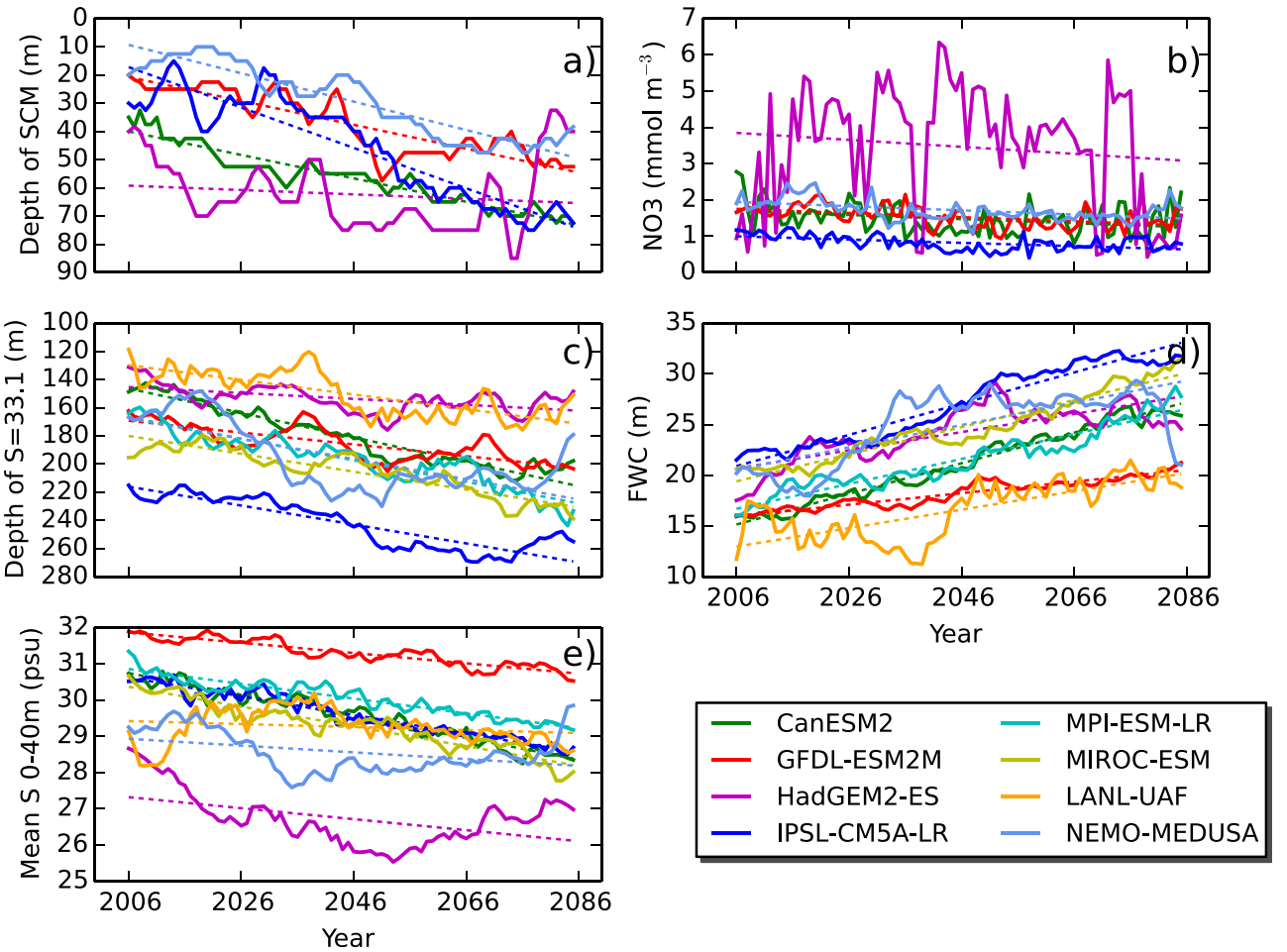

Figure 11. Projected for the years 2006–2085 (a) depth (m) of the SCM (5 year running mean), (b) NO_3 (mmol m^3) at the SCM depth, (c) depth (m) of the 33.1 isohaline, (d) integrated freshwater content (m) as defined in equation (3.2), and (e) mean salinity in the top 40 m (psu). Model data averaged over the area 73°N–79°N and 130°W–150°W.

5.2. The SCM and Stratification

None of the models is able to represent the high-resolution vertical stratification structure in the near surface which is seen in the observations [e.g., *Jackson et al.*, 2010b]. However, most models are able to represent the SCM, as well as its deepening over time. This indicates that the processes affecting the stratification in the near-surface waters, e.g., enhanced warming of the near-surface temperature maximum have limited effect on the projected changes in the SCM. The model intercomparison also shows that some of the characteristic features in the Canada Basin (e.g., changes in the SCM, changes in FWC) are consistent between the coarse resolution ESMs and the corresponding high-resolution ocean model driven with output from the respective ESM. This suggests that large-scale physical processes are responsible for those features. Based on those results the models support the suggestion that enhanced stratification due to addition of freshwater and likely enhanced Ekman pumping [*McLaughlin and Carmack*, 2010], which are represented in the large-scale models, are the main drivers for the deepening of the nitracline and the deepening of the SCM.

Given the proposed link between sea ice melt, freshwater accumulation and deepening of the SCM [*McLaughlin and Carmack*, 2010; *Jackson et al.*, 2010a], and the fact that current ESMs do not represent the rapid sea ice decline seen in the observations [*Stroeve et al.*, 2005, 2012], it is also not surprising that only some models show a deepening in the SCM for the short time period of the observations.

Some model examples suggest that continued thinning of the ice cover might leave the winter ice fragile and too thin to provide a barrier to momentum fluxes. In that case, winter mixing can break up the strong

AGU Journal of Geophysical Research: Oceans 10.1002/2015JC011232

Table 2. Summary of Model Results[a]

Model	Chl-*a* (5 m) Curr./Fut./Trend[b] mg Chl m^{-2}	Chl-*a* (10 m) Curr./Fut./Trend[b] mg Chl m^{-2}	Chl-*a* (200 m) Curr./Fut./Trend[b] mg Chl m^{-2}	Ratio (5–200 m) Curr./Fut./Trend[b]	Ratio (10–200 m) Curr./Fut./Trend[b]	SCM Trend[b] m	NO_3 Trend[b] mmol m^{-3}	S:33.1 Trend[b] m	FWC Trend[b] m
CanESM2	0.23/0.02/−0.003	0.47/0.048/−0.007	7.14/6.79/−0.009	0.033/0.0036/−0.051	0.066/0.007/−0.102	0.42	−0.006	0.87	0.15
GFDL-ESM2M	1.27/0.90/−0.007	2.56/1.81/−0.013	22.28/23.09/0.016	0.057/0.039/−0.034	0.114/0.078/−0.068	0.42	−0.006	0.42	0.06
HadGEM2-ES	0.11/0.32/0.003	0.23/0.65/0.006	13.14/18.13/0.071	0.009/0.018/0.011	0.017/0.035/0.023	0.08	−0.01	0.21	0.09
IPSL-CM5A-LR	1.34/0.66/−0.012	2.68/1.31/−0.025	23.38/20.31/−0.054	0.057/0.032/−0.047	0.115/0.065/−0.093	0.72	−0.005	0.67	0.15
MPI-ESM-LR	2.17/2.13	4.35/4.26	6.14/6.92	0.354/0.308	0.707/0.616			0.76	0.12
MIROC-ESM	0.50/0.77	1.0/1.5	3.41/6.57	0.148/0.117	0.296/0.234			0.63	0.13
LANL-UAF	1.14/0.85	2.29/1.70	6.44/5.85	0.177/0.145	0.356/0.291			0.52	0.09
NEMO-MEDUSA	0.96/0.58/−0.006	1.91/1.16/−0.011	8.68/13.40/0.087	0.110/0.043/−0.111	0.220/0.087/−0.223	0.50	−0.006	0.72	0.11
NAA-CMOC	0.016/0.013	0.033/0.027	5.46/5.77	0.003/0.002	0.006/0.005				

[a]Model averages for integrated Chl-*a* over the upper 5, 10, and 200 m, and ratios (Chl-*a* 5 m integral/Chl-*a* 200 m integral and Chl-*a* 10 m integral/Chl-*a* 200 m) of the water column in current (2006–2025) and future (2066–2085) times, as well as trends of each from 2006 to 2085 (separated by dash: curr./fut./trend) for the ESMs and HROMs used in this study (Table 1). Also provided are the respective trends for the depth of the SCM, NO_3 concentration at the SCM, depth of the S = 33.1 halocline, and the FWC. All data have been averaged over the Canada Basin domain (≈73°N–79°N, 130°W–150°W).

[b]Trends (given as the slope of the regression line) are provided only for models which simulate a SCM and provide time series data. Exceptions are trends of halocline depth and FWC which are provided for all models with time series data. All trends are per year ($year^{-1}$). Positive trends indicate a deepening for the SCM, and increases for FWC, mean salinity, and NO_3 and Chl-*a* concentrations.

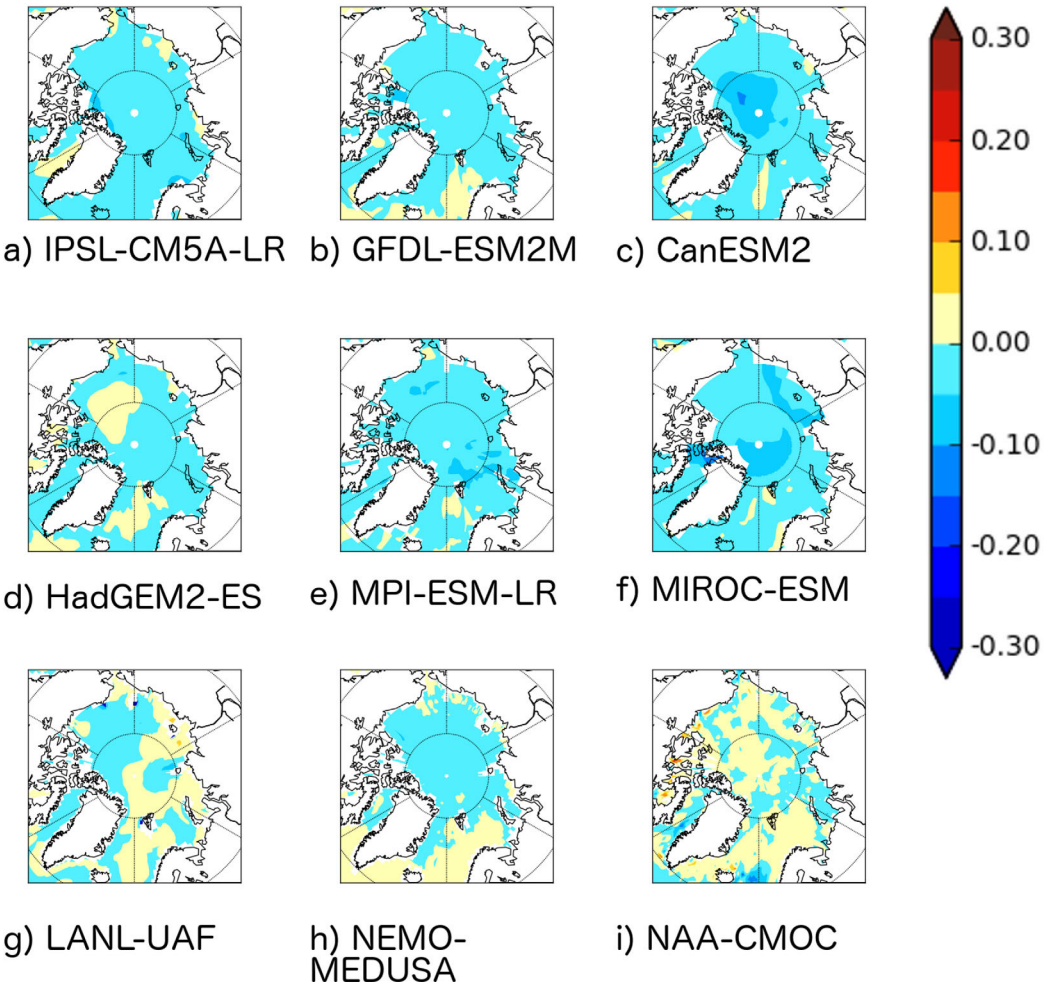

Figure 12. Simulated differences (2066–2085 minus 2006–2026) in the ratio of chlorophyll-a concentration integrated over the upper 5 m versus the 200 m water column of (a) CanESM2, (b) GFDL-ESM2M, (c) HadGEM2-ES, (d) IPSL-CM5A-LR, (e) MPI-ESM-LR, (f) MIROC-ESM, (g) LANL-UAF, (h) NEMO-MEDUSA, and (i) NAA-CMOC. Negative values indicate a decrease of surface Chl-*a* versus integrated Chl-*a*, suggesting a higher contribution of subsurface production.

stratification in the Canada Basin and cause saltier near-surface waters and possibly enhanced nutrient supply. This will be particularly efficient if reduced summer melt due to thin winter ice cover already reduces the stratification.

5.3. Ecosystem Complexity

Model ecosystem parameterizations might cause some inconsistencies among the models as well as biases between models and observations. For example, underestimated grazing might allow high Chl-*a* even with low nutrient values, or the model system might be especially tuned to thrive under low-nutrient conditions. A simplified ecosystem model, e.g., representing only single phytoplankton, zooplankton, and N based nutrient species, does not allow the model to shift from larger to smaller phytoplankton species over time as suggested by *Li et al.* [2009], to represent different depth occupations by different species [*Monier et al.*, 2014], allow preferences for zooplankton species with multiple life stages [*Hunt et al.*, 2014]. Hence, the use of a simple NPZD model might cause the model to represent a very defined SCM, with not much other production or, if tuned differently only represent a surface community. For example, it is possible that the clear SCM feature seen in the CanESM2 and NAA-CMOC models is related to the simpler ecosystem model, with CMOC representing only one phytoplankton species. MIROC also has only one species and shows enhanced surface Chl-*a* only. On the other hand, *Monier et al.* [2014] indicated that SCM communities are most diverse compared to surrounding microbial communities, which might suggest that the conditions at the SCM are

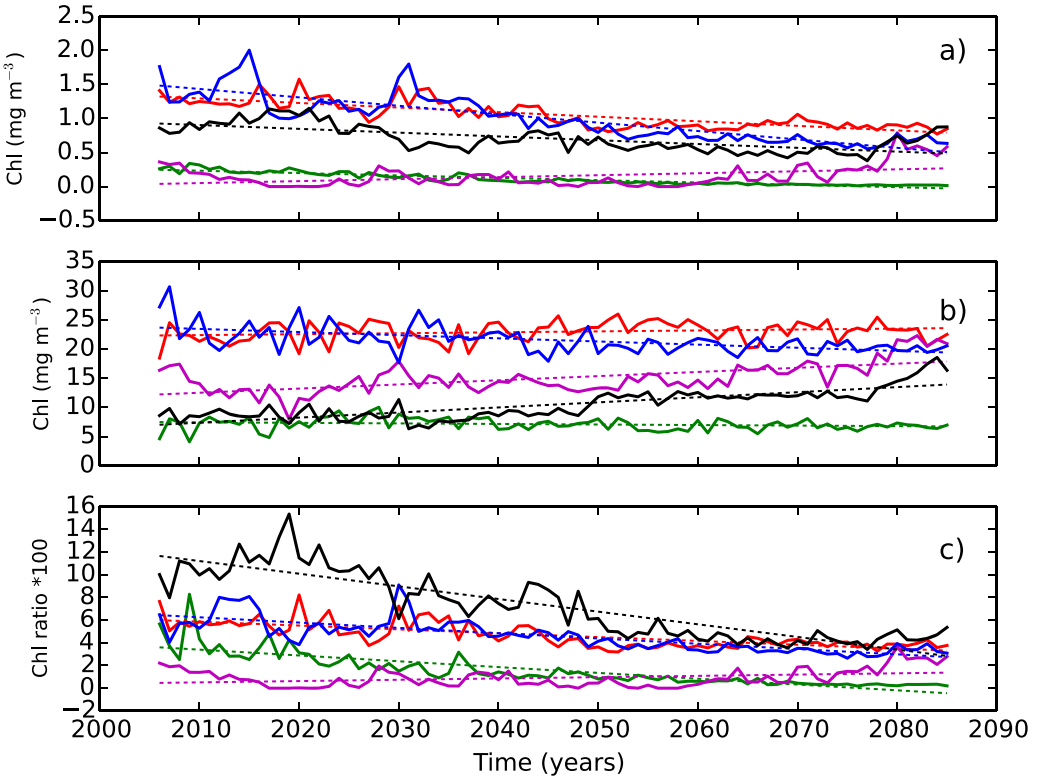

Figure 13. Time series of (a) the chlorophyll-a concentration integrated over the top 5 m and (b) integrated over the upper 200 m. (c) Ratio of Chl-*a* integrated over 5 m versus integrated over 200 m. The model data are averaged over the area 73°N–79°N and 130°W–150°W. Models represented are CanESM2 (green), GFDL-ESM2M (red), HadGEM2-ES (magenta), IPSL-CM5A-LR (blue), NEMO-MEDUSA (black).

favorable enough to allow appropriate representation even in single species models. Another reason for the good correspondence between CanESM2 and the observations could be the relationship to the source water mass. *Steiner et al.* [2014] indicated that the excessive shelf depth in CanESM2 allows the model to retain the vertical structure entering via the Chukchi Sea, while the entering signature is removed in other models where mixing over the complete shelf depth occurs. A direct link between the depth of the SCM and the Pacific layer has been pointed out in *McLaughlin and Carmack* [2010].

5.4. Chl-*a* and Primary Production

The current almost analysis exclusively dealt with Chl-*a*, assuming a general correspondence with phytoplankton growth and hence PP. However, *Cullen* [1982] indicated the relationship between Chl-*a* and phytoplankton biomass to be highly variable (C:Chl-*a* ratio) and cautioned against interpreting vertical Chl-*a* profiles with respect to their ecological significance. Particularly in oligotrophic regions where PP and Chl-*a* concentration are maximal near the nitracline (they refer to the North Pacific central gyre), Chl-*a* concentration is suggested to be a poor indicator of phytoplankton biomass, since the Chl-*a* maximum represents a physiological adaptation to the lower irradiance at depth and the greater availability of nutrients in that stratum affecting the C:Chl ratio. In some regions (e.g., Baffin Bay, Chukchi Sea), the SCM has been found to coincide with the subsurface biomass maximum, but a decoupling between the SCM and the subsurface biomass maximum is identified in other regions [*Martin et al.*, 2010; *Brown et al.*, 2015]. *Coupel et al.* [2015] find an exponential decrease of the PP/Chl-*a* ratio with depth and the SCM occurring much deeper than the PP maximum. *Falkowski and Raven* [2007] indicate that phytoplankton growing at low light may produce 5–10 times as much Chl-*a* as those growing at high light. Indicative of the higher requirement for Chl-*a* production by deep communities to absorb light, the deep SCM shows very low carbon fixation rates, despite the high Chl-*a* concentrations [*Coupel et al.*, 2015]. Observed C:Chl-*a* in the Canada Basin have been found significantly reduced at the SCM versus the surface [*Lee and Whitledge*, 2005; *Brown et al.*, 2015] indicating photoacclimation.

Brown et al. [2015] also found lower biomass in deeper SCMs compared to shallower SCMs due to reduced growth rates in lower light conditions. Most of the models are using variable Chl-*a*:C ratios (Table 1), albeit with slightly different parameterizations and maximum ratios. Models with constant ratios also use different values. While these inconsistencies might be a contributing factor to different Chl-*a* representations among the models, the differences are insufficient to explain the occurrence of a SCM or a lack thereof.

5.5. Ratio of Surface to Integrated Chl-*a*

While the models are consistent in projecting a decreased ratio of surface to integrated Chl-*a* in the future, the contributing factors vary. Some models show a decrease in the surface and some an increase. Most models (7 out of 9) show an increase in subsurface Chl-*a*, although not necessarily linked to the SCM, e.g., two models show subsurface increases without reproducing a SCM. The simulated Chl-*a* concentration at the SCM generally seems to remain fairly constant. However, it is possible that an extension in the open water season would allow the SCM to be sustained for a longer time period. If the SCM shows a slight decrease in depth over the course of the season, longer duration of the SCM could also lead to a broadening of the SCM in the annual mean. In all but one cases, the combined surface and subsurface changes lead to a reduction in the ratio of surface Chl-*a* to integrated Chl-*a* in the Canada Basin. This suggests that the reduction is consistent, even though changes in ratio are small for most areas of the Arctic. Note that the one exception is caused by changes in the last decade of the simulated period, likely due to transition into a new state where sea ice becomes too thin and too fragile to prevent winter mixing and provides too little meltwater to add stability to the stratification. This state might also be reached in other models if warming continues and the models were run out further into the future.

6. Summary

Six ESMs and three higher-resolution ocean-ice-ecosystem models have been analyzed and compared with respect to the evolution of the SCM in the Canada Basin and the ratio of surface to integrated Chl-*a* in a future climate scenario. Observations show a deepening of the SCM before 2010 and stabilizing values in recent years, suggesting an unclear future trend. However, most models indicate a continuation of the observed deepening of the SCM following a deepening of the nitracline until the models reach a new state with seasonal ice-free waters.

We conclude that intermodel differences in the representation of a SCM in the Canada Basin are mainly due to biogeochemical factors: (1) inconsistencies in nutrient availability and (2) differences in the represented ecosystem community structure among the models. On the other hand, intermodel differences in the projected deepening of the SCM in the Canada Basin are likely caused by a variety of physical factors: (1) the different rate of recent and projected sea ice retreat affecting freshwater contribution and stratification, (2) the model's strength of the Beaufort Gyre circulation and consequent accumulation of freshwater in the Canada Basin, and (3) differences in horizontal water mass transport, possibly related to vertical resolution on the shelves.

The ratio of near-surface Chl-*a* to the depth-integrated Chl-*a* is projected to decrease in most areas of the Arctic Ocean, indicating an enhanced contribution of subsurface Chl-*a*. Exceptions are some shelf areas and situations when the ice cover thins enough to permanently break the stratification and allow nutrient mixing into the near-surface ocean. The results confirm that production algorithms determining vertically integrated Chl-*a* from near-surface Chl-*a* need to represent the characteristic SCM in the Arctic, but at this point it is not suggested that algorithms need to be further adjusted to properly represent enhanced subsurface production in the future.

However, several factors might affect how and if the models can adequately represent the evolution of surface versus subsurface production and should be addressed in future work. Improvements in nutrient databases and respective model representations of the Arctic are necessary to avoid the large discrepancies currently inherent to the models. An additional limitation here is that much CMIP5 output were only archived and made available at annual frequency, which limits analysis in highly seasonal regions like the Arctic. We would advocate that future activities, such as its successor project CMIP6, provide output at higher temporal

frequency (e.g., monthly) for variables with high seasonality to allow a more complete understanding of the Arctic. Further studies should also include the analysis of effects from ecosystems with different complexity with respect to the representation of plankton growth at different depths and their ability to capture shifts in future climates as well as the relationship between Chl-*a*, PP, and organic carbon.

Acknowledgments

We acknowledge the World Climate Research Program's Working Group on Coupled Modeling, which is responsible for CMIP5, and we thank the respective climate modeling groups for producing and making available their model output. For CMIP5, the U.S. Department of Energy's Program for Climate Model Diagnosis and Intercomparison provides coordinating support and led development of software infrastructure in partnership with the Global Organization for Earth System Science Portals. We also acknowledge the staff of PCMDI and the other data repositories, and the developers of the CDO software. Mooring and hydrographic data were collected and made available by the Beaufort Gyre Exploration Program based at the Woods Hole Oceanographic Institution (http://www.whoi.edu/beaufortgyre) in collaboration with researchers from Fisheries and Oceans Canada at the Institute of Oceans Sciences. We thank two anonymous reviewers for constructive comments on the manuscript, Neil Swart for his help in processing various model data fields, and Sarah Zimmerman for updating the basin-averaged observational time series. The publication contributes to the Forum for Arctic Modeling and Observational Synthesis (FAMOS) and we thank FAMOS for providing an opportunity to discuss and present ideas leading to this publication at the FAMOS meetings. The work has been funded by Fisheries and Oceans Canada via the Aquatic Climate Change Adaptation Services Program (ACCASP) and Environment Canada.

References

Alkire, M., J. Morison, and R. Andersen (2015), Variability in the meteoric water, sea-ice melt, and Pacific water contributions to the central Arctic Ocean, 2000-2014, *J. Geophys. Res. Oceans*, *120*, 1573–1598, doi:10.1002/2014JC010023.

Ardyna, M., M. Babin, M. Gosselin, E. Devred, S. Bélanger, A. Matsuoka, and J.-E. Tremblay (2013), Parameterization of vertical chlorophyll a in the Arctic Ocean: Impact of the subsurface chlorophyll maximum on regional, seasonal, and annual primary production estimates, *Biogeosciences*, *10*, 4383–4404, doi:10.5194/bg-10-4383-2013.

Arora, V. K., J. Scinocca, G. J. Boer, J. R. Christian, K. L. Denman, G. M. Flato, V. V. Kharin, W. G. Lee, and W. J. Merryfield (2011), Carbon emission limits required to satisfy future representative concentration pathways of greenhouse gases, *Geophys. Res. Lett.*, *38*, L05805, doi:10.1029/2010GL046270.

Arrigo, K., P. Matrai, and G. Dijken (2011), Primary productivity in the Arctic Ocean: Impacts of complex optical properties and subsurface chlorophyll maxima on large-scale estimates, *J. Geophys. Res.*, *116*, C11022, doi:10.1029/2011JC007273.

Aumont, O., E. Maier-Reimer, S. Blain, and P. Monfray (2003), An ecosystem model of the global ocean including Fe, Si, P colimitations, *Global Biogeochem. Cycles*, *17*(2), 1060, doi:10.1029/2001GB001745.

Brown, Z., K. Lowry, M. Palmer, G. van Dijken, M. Mills, R. Pickart, and K. Arrigo (2015), Characterizing the subsurface chlorophyll a maximum in the Chukchi sea and Canada Basin, *Deep Sea Res., Part II*, *118*, 88–104.

Carmack, E. C., and D. C. Chapman (2003), Wind-driven shelf/basin exchange on an Arctic shelf: The joint roles of ice cover extent and shelf-break bathymetry, *Geophys. Res. Lett.*, *30*(14), 1778, doi:10.1029/2003GL017526.

Carmack, E. C., R. W. MacDonald, and J. Papadakis (1989), Water mass structure and boundaries in the Mackenzie shelf estuary, *J. Geophys. Res.*, *94*, 18,043–18,055, doi:10.1029/JC094iC12p18043.

Carmack, E. C., R. W. MacDonald, and S. Jasper (2004), Phytoplankton productivity on the Canadian shelf of the Beaufort Sea, *Mar. Ecol. Prog. Ser.*, *277*, 37–50.

Christian, J. R., et al. (2010), The global carbon cycle in the Canadian earth system model (CanESM1): Preindustrial control simulation, *J. Geophys. Res.*, *115*, G03014, doi:10.1029/2008JG000920.

Collins, W. J., et al. (2011), Development and evaluation of an earth-system model—HadGEM2, *Geosci. Model Dev.*, *4*(4), 1051–1075, doi:10.5194/gmd-4-1051-2011.

Coupel, P., D. Ruiz-Pino, M. Sicre, J. Chen, S. Lee, N. Schiffrine, H. Li, and J. Gascard (2015), The impact of freshening on phytoplankton production in the Pacific Arctic Ocean, *Prog. Oceanogr.*, *131*, 113–125, doi:10.1016/j.pocean.2014.12.003.

Cullen, J. (1982), The deep chlorophyll maximum: Comparing vertical profiles of chlorophyll a, *Can. J. Fish. Aquat. Sci.*, *39*, 791–803.

Deal, C., S. Elliott, M. Jin, E. Hunke, M. Maltrud, and N. Jeffery (2011), Large scale modeling of primary production and ice algal biomass within Arctic sea ice, *J. Geophys. Res.*, *116*, C07004, doi:10.1029/2010JC006409.

Dufresne, J.-L., et al. (2013), Climate change projections using the IPSL-CM5 earth system model: From CMIP3 to CMIP5, *Clim. Dyn.*, *40*(9), 2123–2165, doi:10.1007/s00382-012-1636-1.

Dunne, J. P., et al. (2012), GFDLs ESM2 global coupled climate-carbon earth system models. Part I: Physical formulation and baseline simulation characteristics, *J. Clim.*, *25*(19), 6646–6665.

Dunne, J. P., et al. (2013), GFDLs ESM2 global coupled climate-carbon earth system models. Part II: Carbon system formulation and baseline simulation characteristics, *J. Clim.*, *26*(7), 2247–2267, doi:10.1175/JCLI-D-12-00150.1.

Falkowski, P., and J. Raven (2007), *Aquatic Photosynthesis*, Princeton Univ. Press, Princeton, N. J.

Geider, R., H. MacIntyre, and T. Kana (1996), A dynamic model of photoadaptation in phytoplankton, *Limnol. Oceanogr.*, *41*, 1–15.

Geider, R., H. MacIntyre, and T. Kana (1997), A dynamic model of phytoplankton growth and acclimation: Responses of the balanced growth rate and chlorophyll a: Carbon ratio to light, nutrient-limitation and temperature, *Mar. Ecol. Prog. Ser.*, *148*, 187–200.

Giorgetta, M., et al. (2013), Climate and carbon cycle changes from 1850 to 2100 in MPI-ESM simulations for the coupled model intercomparison project phase 5, *J. Adv. Model. Earth Syst.*, *5*, 572–597, doi:10.1002/jame.20038.

HadGEM2 Development Team (2011), The HadGEM2 family of met office unified model climate configurations, *Geosci. Model Dev.*, *4*(3), 723–757, doi:10.5194/gmd-4-723-2011.

Hill, V., et al. (2013), Synthesis of integrated primary production in the Arctic Ocean: II. In situ and remotely sensed estimates, *Prog. Oceanogr.*, *110*, 107–125.

Hu, X., and P. Myers (2013), A Lagrangian view of Pacific water inflow pathways in the Arctic Ocean during model spin-up, *Ocean Modell.*, *71*, 66–80, doi:10.1016/j.ocemod.2013.06.007.

Hu, X., and P. Myers (2014), Changes to the Canadian Arctic Archipelago sea ice and freshwater fluxes in the 21st century under the IPCC A1B climate scenario, *Atmos. Ocean*, *52*, 331–350, doi:10.1080/07055900.2014.942592.

Hunt, B., R. Nelson, B. Williams, F. McLaughlin, K. Young, K. Brown, S. Vagle, and E. Carmack (2014), Zooplankton community structure and dynamics in the Arctic Canada Basin during a period of intense environmental change (2004-2009), *J. Geophys. Res. Oceans*, *119*, 2518–2538, doi:10.1002/2013JC009156.

Ilyina, T., K. D. Six, J. Segschneider, E. Maier-Reimer, H. Li, and I. Nunez-Riboni (2013), The global ocean biogeochemistry model HAMOCC: Model architecture and performance as component of the MPI-earth system model in different CMIP5 experimental realizations, *J. Adv. Model. Earth Syst.*, *5*, 287–315, doi:10.1002/jame.20017.

Jackson, J., S. Allen, E. Carmack, and F. McLaughlin (2010a), Suspended particles in the Canada Basin from optical and bottle data, 2003-2008, *Ocean Sci.*, *6*, 799–813, doi:10.5194/os-6-799-2010.

Jackson, J., E. Carmack, F. McLaughlin, S. Allen, and R. Ingram (2010b), Identification, characterization, and change of the near-surface temperature maximum in the Canada Basin, 1993-2008, *J. Geophys. Res.*, *115*, C05021, doi:10.1029/2009JC005265.

Jackson, J., S. Allen, F. McLaughlin, R. Woodgate, and E. Carmack (2011), Changes to the near-surface waters in the Canada Basin, Arctic Ocean from 1993-2009: A basin in transition, *J. Geophys. Res.*, *116*, C10008, doi:10.1029/2011JC007069.

Jackson, J. M., W. J. Williams, and E. C. Carmack (2012), Winter sea-ice melt in the Canada Basin, Arctic Ocean, *Geophys. Res. Lett.*, *39*, L03603, doi:10.1029/2011GL050219.

Jin, M., C. J. Deal, J. Wang, K. H. Shin, N. Tanaka, T. E. Whitledge, S. H. Lee, and R. R. Gradinger (2006), Controls of the landfast ice-ocean ecosystem offshore Barrow, Alaska, *Ann. Glaciol.*, *44*, 63–72.
Jin, M., C. Deal, J. Wang, V. Alexander, R. Gradinger, S. Saitoh, T. Iida, Z. Wan, and P. Stabeno (2007), Ice-associated phytoplankton blooms in the southeastern Bering Sea, *Geophys. Res. Lett.*, *34*, L06612, doi:10.1029/2006GL028849.
Jin, M., C. Deal, S. Lee, S. Elliott, E. Hunke, M. Maltrud, and N. Jeffery (2012a), Investigation of Arctic sea ice and ocean primary production for the period 1992-2007 using a 3-D global ice-ocean ecosystem model, *Deep Sea Res., Part II*, *81*, 28–35, doi:10.1016/j.dsr2.2011.06.003.
Jin, M., J. Hutchings, Y. Kawaguchi, and T. Kikuchi (2012b), Ocean mixing with lead-dependent subgrid scale brine rejection parameterization in a climate model, *J. Ocean Univ. China*, *11*(4), 473–480, doi:10.1007/s11802-012-2094-4.
Kawamiya, M., M. J. Kishi, and N. Suginohara (2000), An ecosystem model for the North Pacific embedded in a general circulation model, part I: Model description and characteristics *of spatial distributions of biological variables, J. Mar. Syst.*, *25*, 129–157.
Lee, S., and T. Whitledge (2005), Primary and new production in the deep Canada Basin during summer 2002, *Polar Biol.*, *28*, 190–197.
Li, W., F. McLaughlin, and C. Lovejoy (2009), Smallest algae thrive as the Arctic Ocean freshens, *Science*, *326*, 539, doi:10.1126/science.1179798.
Lovejoy, C. (2012), Polar marine microbiology, in *Polar Microbiology: Life in a Deep Freeze*, pp. 1–17, ASM Press, Washington, D. C.
Macdonald, R., M. O'Brien, E. Carmack, R. Pearson, F. McLaughlin, D. Sieberg, J. Barwell-Clarke, D. W. Paton, and D. Tuele (1995), Physical and chemical data collected in the Beaufort, Chukchi and East Siberian Seas, *Can. Data Rep. Hydrogr. Ocean Sci. 139*, 287 pp., Gov. of Can., Ottawa.
Madec, G. (2008), NEMO reference manual, ocean dynamic component: NEMO-OPA, *Tech. Rep. 27*, Note du Pole de Modlisation, Inst. Pierre Si- mon Laplace, Paris, France.
Martin, J., J.-E. Tremblay, J. Gagnon, G. Tremblay, A. Lapoussière, C. Jose, M. Poulin, M. Gosselin, Y. Gratton, and C. Michel (2010), Prevalence, structure and properties of subsurface chlorophyll maxima in Canadian Arctic water, *Mar. Ecol. Prog. Ser.*, *412*, 69–84, doi:10.3354/meps08666.
Martin, J., D. Dumont, and J.-E. Tremblay (2013), Contribution of subsurface chlorophyll maxima to primary production in the coastal Beaufort Sea (Canadian Arctic): A model assessment, *J. Geophys. Res. Oceans*, *118*, 5873–5886, doi:10.1002/2013JC008843.
Maykut, G., and M. McPhee (1995), Solar heating of the Arctic mixed layer, *J. Geophys. Res.*, *100*, 24,691–24,702, doi:10.1029/95JC02554.
McLaughlin, F., and E. Carmack (2010), Deepening of the nutricline and chlorophyll maximum in the Canada Basin interior, 2003-2009, *Geophys. Res. Lett.*, *37*, L246902, doi:10.1029/2010GL045459.
McLaughlin, F., E. Carmack, R. Macdonald, and J. Bishop (1996), Physical and geochemical properties across the Atlantic/Pacific front in the southern Canadian Basin, *J. Geophys. Res.*, *101*, 1183–1197, doi:10.1029/95JC02634.
McLaughlin, F., E. Carmack, R. Macdonald, A. J. Weaver, and J. Smith (2002), The Canada Basin 1989-1995: Upstream events and far-field effects of the Barents Sea, *J. Geophys. Res.*, *107*(C7), 2156, doi:10.1029/2001JC000904.
McLaughlin, F., E. C. Carmack, S. Zimmerman, D. Sieberg, L. White, J. Barwell-Clarke, M. Steel, and W. K. W. Li (2008), Physical and chemical data from the Canada Basin, August, 2004, *Can. Data Rep. Hydrogr. Ocean Sci. 140*, 185 pp., Gov. of Can., Ottawa.
McLaughlin, F., E. Carmack, A. Proshutinsky, R. Krishfield, C. Guay, M. Yamamoto-Kawai, J. Jackson, and B. Williams (2011), The rapid response of the Canada Basin to climate forcing—From bellwether to alarm bells, *Oceanography*, *24*(3), 146–159.
McPhee, M., A. Proshutinsky, J. Morison, M. Steele, and M. Alkire (2009), Rapid change in freshwater content of the Arctic Ocean, *Geophys. Res. Lett.*, *36*, L10602, doi:10.1029/2009GL037525.
Monier, A., J. Comte, M. Babin, A. Forest, A. Matsuoka, and C. Lovejoy (2014), Oceanographic structure drives the assembly processes of microbial eukaryotic communities, *ISME J.*, *9*(4), 990–1002.
Moore, J., S. Doney, and K. Lindsay (2004), Upper ocean ecosystem dynamics and iron cycling in a global three-dimensional model, *Global Biogeochem. Cycles*, *18*, GB4028, doi:10.1029/2004GB002220.
Moore, J. K., S. C. Doney, D. M. Glover, and I. Y. Fung (2002), Iron cycling and nutrient-limitation patterns in surface waters of the world ocean, *Deep Sea Res., Part II*, *49*, 463–507.
Morel, A., and J. Berthon (1989), Surface pigments, algal biomass profiles, and potential production of the euphotic layer: Relationships reinvestigated in view of remote-sensing applications, *Limnol. Oceanogr.*, *34*, 1545–1562.
Moss, R. H., et al. (2010), The next generation of scenarios for climate change research and assessment, *Nature*, *463*, 747–756, doi:10.1038/nature08823.
Mundy, C., et al. (2009), Contribution of under-ice primary production to an ice-edge upwelling phytoplankton bloom in the Canadian Beaufort Sea, *Geophys. Res. Lett.*, *36*, L17601, doi:10.1029/2009GL038837.
Oschlies, A. (2001), Model-derived estimates of new production: New results point towards lower values, *Deep Sea Res., Part II*, *48*, 2173–2197.
Palmer, J., and I. Totterdell (2001), Production and export in a global ocean ecosystem model, *Deep Sea Res., Part I*, *48*, 1169–1198.
Peralta-Ferriz, C., and R. Woodgate (2015), Seasonal and interannual variability of pan-Arctic surface mixed layer properties from 1979 to 2012 from hydrographic data, and the dominance of stratification for multiyear mixed layer depth shoaling, *Prog. Oceanogr.*, *134*, 19–53, doi:10.1016/j.pocean.2014.12.005.
Polyakov, I., A. Pnyushkov, R. Rember, L. Padman, E. Carmack, and J. Jackson (2013), Winter convection transports Atlantic water heat to the surface layer in the eastern Arctic Ocean, *J. Phys. Oceanogr.*, *43*, 2142–2155, doi:10.1175/JPO-D-12-0169.1.
Popova, E., A. Yool, A. Coward, F. Dupont, C. Deal, S. Elliott, E. Hunke, M. Jin, M. Steele, and J. Zhang (2012), What controls primary production in the Arctic Ocean? Results from an intercomparison of five general circulation models with biogeochemistry, *J. Geophys. Res.*, *117*, C00D12, doi:10.1029/2011JC007112.
Popova, E., A. Yool, Y. Aksenov, A. Coward, and T. Anderson (2014), Regional variability of acidification in the Arctic: A sea of contrasts, *Biogeosciences*, *11*, 293–308, doi:10.5194/bg-11-293-2014.
Popova, E. E., et al. (2010), Control of primary production in the Arctic by nutrients and light: Insights from a high resolution ocean general circulation model, *Biogeosciences*, *7*, 3569–3591, doi:10.5194/bg-7-3569-2010.
Popova, E. E., A. Yool, Y. Aksenov, and A. C. Coward (2013), Role of advection in Arctic Ocean lower trophic dynamics: A modeling perspective, *J. Geophys. Res. Oceans*, *118*, 1571–1586, doi:10.1002/jgrc.20126.
Proshutinsky, A., R. Bourke, and F. McLaughlin (2002), The role of the Beaufort gyre in Arctic climate variability: Seasonal to decadal climate scales, *Geophys. Res. Lett.*, *29*(23), 2100, doi:10.1029/2002GL015847.
Rabe, B., M. Karcher, U. Schauer, J. Toole, R. Krishfield, S. Pisarev, F. Kauker, R. Gerdes, and T. Kikuchi (2011), An assessment of Arctic Ocean freshwater content changes from the 1990s to the 2006-2008, *Deep Sea Res., Part I*, *58*, 173–185.
Scinocca, J., V. Kharin, Y. Jiao, M. Qian, M. Lazare, L. Solheim, and G. Flato (2016), Coordinated global and regional climate modelling, *J. Clim.*, *29*, 17–35.

Six, K. D., and E. Maier-Reimer (1996), Effects of plankton dynamics on seasonal carbon fluxes in an ocean general circulation model, *Global Biogeochem. Cycles*, *10*, 559–583.
Steele, M., J. Morison, W. Ermold, I. Rigor, M. Ortmeyer, and K. Shimada (2004), Circulation of summer Pacific halocline water in the Arctic Ocean, *J. Geophys. Res.*, *109*, C02027, doi:10.1029/2003JC002009.
Steiner, N., et al. (2004), Comparing modeled streamfunction, heat and freshwater content in the Arctic Ocean, *Ocean Modell.*, *6*, 265–284.
Steiner, N., et al. (2015), Observed trends and climate projections affecting marine ecosystems in the Canadian Arctic, *Environ. Rev.*, *23*(2), 191–239, doi:10.1139/er-2014-0066.
Steiner, N. S., J. R. Christian, K. Six, A. Yamamoto, and M. Yamamoto-Kawai (2014), Future ocean acidification in the Canada Basin and surrounding Arctic Ocean from CMIP5 earth system models, *J. Geophys. Res. Oceans*, *119*, 332–347, doi:10.1002/2013JC009069.
Stroeve, J. C., M. C. Serreze, F. Fetterer, T. Arbetter, W. Meier, J. Maslanik, and K. Knowles (2005), Tracking the Arctic's shrinking ice cover: Another extreme September minimum in 2004, *Geophys. Res. Lett.*, *32*, L04501, doi:10.1029/2004GL021810.
Stroeve, J. C., V. Kattsov, A. Barrett, M. Serreze, T. Pavlova, M. Holland, and W. N. Meier (2012), Trends in Arctic sea ice extent from CMIP5, CMIP3 and observations, *Geophys. Res. Lett.*, *39*, L16502, doi:10.1029/2012GL052676.
Timmermann, R., H. Goosse, G. Madec, T. Fichefet, C. Ethe, and V. Duliere (2005), On the representation of high latitude processes in the ORCA-LIM global coupled sea ice-ocean model, *Ocean Modell.*, *8*, 175–201, doi:10.1016/j.ocemod.2003.12.009.
Timmermans, M.-L. (2015), The impact of stored solar heat on Arctic sea-ice growth, *Geophys. Res. Lett.*, *42*, 6399–6406, doi:10.1002/2015GL064541.
Timmermans, M.-L., S. Cole, and J. Toole (2012), Horizontal density structure and restratification of the Arctic Ocean surface layer, *J. Phys. Oceanogr.*, *42*(2), 659–668, doi:10.1175/JPO-D-11-0125.1.
Timmermans, M.-L., et al. (2014), Mechanisms of pacific summer water variability in the Arctic's central Canada Basin, *J. Geophys. Res. Oceans*, *119*, 7523–7548, doi:10.1002/2014JC010273.
Tremblay, J.-E., K. Simpson, J. Martin, L. Miller, Y. Gratton, D. Barber, and N. M. Price (2008), Vertical stability and the annual dynamics of nutrients and chlorophyll fluorescence in the coastal, southeast Beaufort Sea, *J. Geophys. Res.*, *113*, C07S90, doi:10.1029/2007JC004547.
Tremblay, J.-E., et al. (2011), Climate forcing multiplies biological productivity in the coastal Arctic Ocean, *Geophys. Res. Lett.*, *38*, L18604, doi:10.1029/2011GL048825.
Uitz, J., H. Claustre, A. Morel, and S. Hooker (2006), Vertical distribution of phytoplankton communities in open ocean: An assessment based on surface chlorophyll, *J. Geophys. Res.*, *111*, C08005, doi:10.1029/2005JC003207.
Vancoppenolle, M., L. Bopp, C. Madec, J. Dunne, T. Ilyina, P. Halloran, and N. Steiner (2013), Future Arctic primary productivity from CMIP5 simulations: Uncertain outcome, but consistent mechanisms, *Global Biogeochem. Cycles*, *27*, 605–619, doi:10.1002/gbc.20055.
Watanabe, S., et al. (2011), MIROC-ESM 2010: Model description and basic results of CMIP5-20c3m experiments, *Geosci. Model Dev.*, *4*(4), 845–872, doi:10.5194/gmd-4-845-2011.
Yool, A., E. Popova, A. Coward, D. Bernie, and T. Anderson (2013a), Climate change and ocean acidification impacts on lower trophic levels and the export of organic carbon to the deep ocean, *Biogeosciences*, *10*, 5831–5854, doi:10.5194/bg-10-5831-2013.
Yool, A., E. E. Popova, and T. R. Anderson (2013b), MEDUSA-2.0: An intermediate complexity biogeochemical model of the marine carbon cycle for climate change and ocean acidification studies, *Geosci. Model Dev.*, *6*, 1767–1811, doi:10.5194/gmd-6-1767-2013.
Zahariev, K., J. Christian, and K. Denman (2008), A global ocean carbon model with parameterizations of iron limitation, calcification and N_2 fixation; preindustrial, historical and fertilization simulations, *Prog. Oceanogr.*, *77*(1), 56–82.